AD_____

Award Number: DAMD17-98-1-8511

TITLE: A Novel High Resolution Positron Emission Tomography
         System for Measurement of Bone Metabolism

PRINCIPAL INVESTIGATOR: John A. Correia, Ph.D.

CONTRACTING ORGANIZATION: Massachusetts General Hospital
                          Boston, Massachusetts 02114

REPORT DATE: September 2000

TYPE OF REPORT: Annual

PREPARED FOR: U.S. Army Medical Research and Materiel Command
               Fort Detrick, Maryland 21702-5012

DISTRIBUTION STATEMENT: Approved for public release;
                        Distribution unlimited

The views, opinions and/or findings contained in this report are
those of the author(s) and should not be construed as an official
Department of the Army position, policy or decision unless so
designated by other documentation.

20010216 029

REPORT DOCUMENTATION PAGE

UMB No. 074-0188

1. AGENCY USE ONLY (Leave blank)	2. REPORT DATE September 2000	3. REPORT TYPE AND DATES COVERED Annual (1 Sep 99 - 31 Aug 00)

4. TITLE AND SUBTITLE

A Novel High Resolution Positron Emission Tomography
System for Measurement of Bone Metabolism

5. FUNDING NUMBERS
DAMD17-98-1-8511

6. AUTHOR(S)

John A. Correia, Ph.D.

7. PERFORMING ORGANIZATION NAME(S) AND ADDRESS(ES)

Massachusetts General Hospital

Boston, Massachusetts 02114

E-MAIL: correia@petw6.mgh.harvard.edu

**8. PERFORMING ORGANIZATION
REPORT NUMBER**

9. SPONSORING / MONITORING AGENCY NAME(S) AND ADDRESS(ES)

U.S. Army Medical Research and Materiel Command
Fort Detrick, Maryland 21702-5012

**10. SPONSORING / MONITORING
AGENCY REPORT NUMBER**

11. SUPPLEMENTARY NOTES

Report contains color graphics.

12a. DISTRIBUTION / AVAILABILITY STATEMENT
Approved for public release; Distribution unlimited

12b. DISTRIBUTION CODE

13. ABSTRACT *(Maximum 200 Words)*

14. SUBJECT TERMS

15. NUMBER OF PAGES
40

16. PRICE CODE

17. SECURITY CLASSIFICATION OF REPORT Unclassified	18. SECURITY CLASSIFICATION OF THIS PAGE Unclassified	19. SECURITY CLASSIFICATION OF ABSTRACT Unclassified	20. LIMITATION OF ABSTRACT Unlimited

FOREWORD

Opinions, interpretations, conclusions and recommendations are those of the author and are not necessarily endorsed by the U.S. Army.

___ Where copyrighted material is quoted, permission has been obtained to use such material.

___ Where material from documents designated for limited distribution is quoted, permission has been obtained to use the material.

___ Citations of commercial organizations and trade names in this report do not constitute an official Department of Army endorsement or approval of the products or services of these organizations.

X In conducting research using animals, the investigator(s) adhered to the "Guide for the Care and Use of Laboratory Animals," prepared by the Committee on Care and use of Laboratory Animals of the Institute of Laboratory Resources, national Research Council (NIH Publication No. 86-23, Revised 1985).

N/A For the protection of human subjects, the investigator(s) adhered to policies of applicable Federal Law 45 CFR 46.

N/A In conducting research utilizing recombinant DNA technology, the investigator(s) adhered to current guidelines promulgated by the National Institutes of Health.

N/A In the conduct of research utilizing recombinant DNA, the investigator(s) adhered to the NIH Guidelines for Research Involving Recombinant DNA Molecules.

N/A In the conduct of research involving hazardous organisms, the investigator(s) adhered to the CDC-NIH Guide for Biosafety in Microbiological and Biomedical Laboratories.

John A. Correia, Ph.D.

TABLE OF CONTENTS:

II. - REPORT BODY:

A. - Introduction:

The overall purposes of this project are :

1. To design and develop an instrument for high resolution PET imaging of the long bones.
2. Demonstrate the use of this device in an experimental protocol to assess estrogen therapy for osteoporosis in a monkey model.

The main thrust of the second year's work was to complete design studies for the proposed PET instrument, construct the instrument and begin imaging studies in monkey bone. Several approaches were used. First, computational and simulation studies begun in the first year were completed, secondly, physical characterization of the prototype device was completed. Data acquisition and analysis software development have also been continued using the prototype. The final design for the imaging device was generated and construction of the device has been undertaken (expected completion by November, 2000). Preliminary animal imaging studies using the prototype have been begun. The details of the work are described in the following sections and in the publications of the Appendix.

B. - Background:

PET (positron emission tomography) imaging is a nuclear medicine technique for measuring quantitative regional physiology and biochemistry in intact animals and humans. The penetrating radiation resulting from positron decay is in the form of two 511 keV photons which are time-correlated and leave the site of the decay in approximately opposite directions. PET imaging devices are designed to detect these photon-pairs as coincidence events. Detection of the photon pairs can be done with high sensitivity relative to other nuclear methods due to the spatial discrimination of coincidence detection. Also, with coincidence detection physical effects such as source self-absorption and photon scatter can be fully corrected. Application of these corrections makes possible quantitative measurement radioactivity distributions. Large-scale PET devices (for human and large animal imaging) are highly evolved and commercially available. The frontier in PET imaging instrumentation lies in developing high resolution, small-scale devices for imaging small animals or, in the case of this work,

4

extremities. The advent of new radiation-detector materials, particularly new scintillators such as Lutetium Orthosilicate (LSO), has made it possible to build such a small-scale device in practice.

The first year's work emphasized the design of an instrument for imaging primate extremities (and possibly human extremities in the future). The approach was to carry out simulation studies of physical and instrument factors as well as design and feasibility experiments to optimize the system design. Then a prototype instrument was constructed as an experimental platform for development of detector module designs, electronics, software for coincidence identification, and for physical imaging studies. The second year's work, the subject of this report, consisted mainly of construction of the final device and associated software and the initial application of the device in animal studies. As an ancillary project related to the main aim of developing a device for bone imaging, design studies for a volumetric (multi-planar) detector have been carried out, a prototype detector module constructed and physical evaluation experiments begun.

C. System Specifications and Construction Progress:

During the first year a prototype instrument was constructed and evaluated. Our intent was threefold. First, to gain knowledge about the limitations of the design, secondly, to evaluate hardware designs developed for the prototype and incorporate them into the final instrument, and thirdly to use software developed for the prototype as a basis for software design for the final instrument. The modifications introduced, discussed in more detail below, include increasing the size of the LSO crystal elements in both width (from 1 to 1.2 mm) and depth (from 5 to 7mm). These changes yield considerably better detector-element performance at a best resolution of 1.2 mm and more than a factor of two improvement in sensitivity. The diameter of the instrument was increased from 12 to 15 cm in order to accommodate larger objects and to keep resolution variation with radius the same as in the prototype. The properties of the prototype and final instruments are summarized in Table I. More detailed discussions of the final system are given in the following sections.

The final system is currently being assembled and is expected to be operational by the end of November, 2000. At the time of this writing: (1) all design studies are completed; photomultiplier tubes have been tested and mounted in the gantry; detector crystals have been cut to size and blocks are

5

being assembled; gantry parts have been constructed and partially assembled; software modules for system calibration, data collection, reconstruction, image display and manipulation, object motion, and data storage have been written and are being integrated. Figure 1 below shows several photographs of the instrument and components during assembly.

Table I: Properties of Prototype and Final Instruments

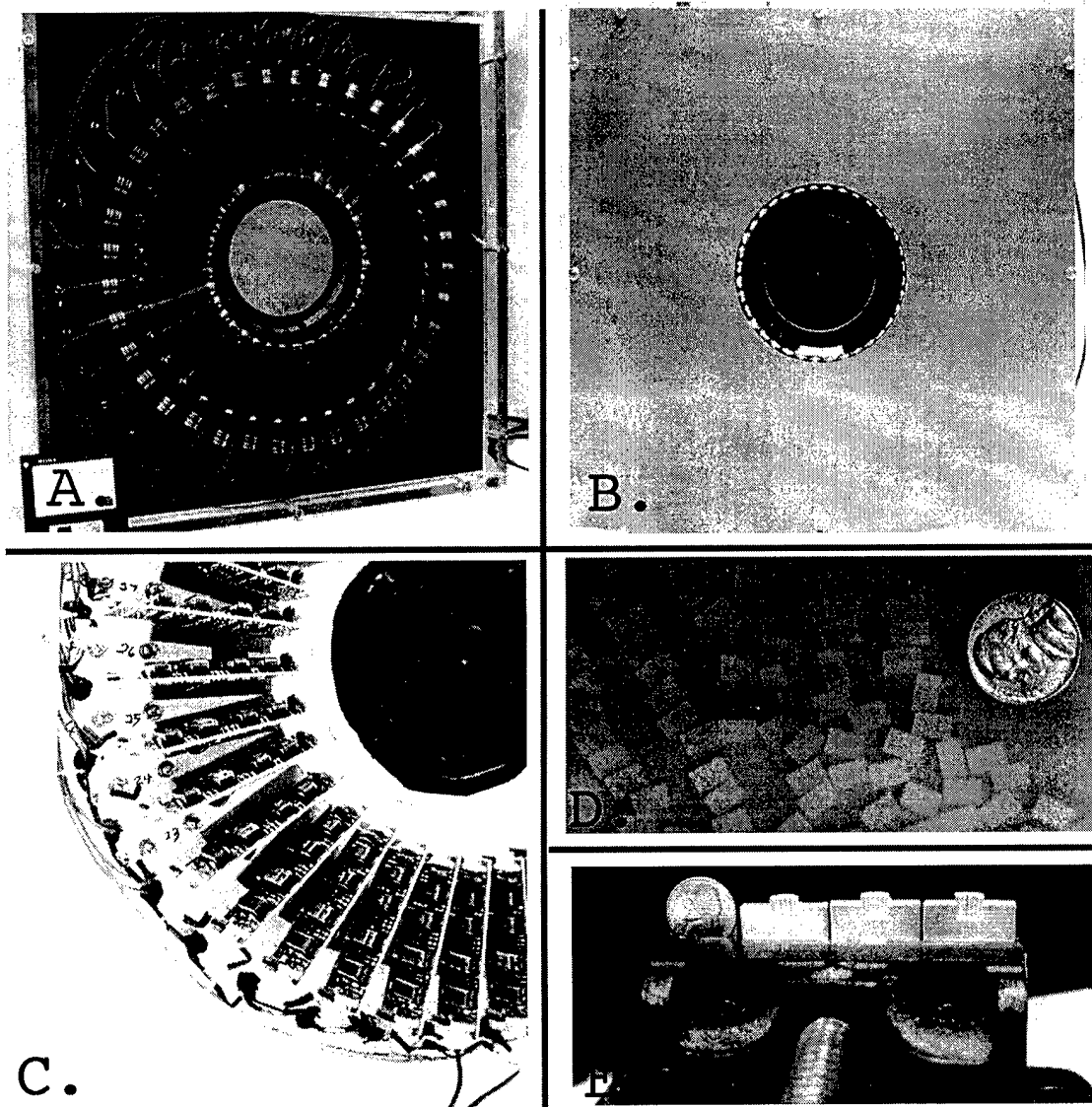| PARAMETER	PROTOTYPE	FINAL
Number of Planes	1	1
Detector Diameter	12 cm	14.7 cm
Crystals	360 LSO	360 LSO
Crystal Dimensions	1x4.5x5 mm	1.2x4.5x7 mm
PMT's/Blocks	30	36
Radial Resolution	1.18mm center 1.6mm @ 2.5 cm Radius	1.2mm center 1.7 mm @ 2.5 cm Radius
Axial Resolution	0.15-0.4 cm	0.15-0.4 cm
Field of View	6 cm	8 cm
Sensitivity-Point	30 cps/uCi	>60 cps/uCi

Figure 1: Photographs of the final system under construction: A. Gantry rear without cover showing phototubes. 3.5" disk shown for scale. B. Gantry front. Tips of phototubes and several detector blocks white) visible. C. Close-up of rear of gantry, cover in place and preamplifier boards mounted. D. LSO crystals cut to size. E. Assembly of blocks. Center 5 crystals being glued in aluminum jigs.

D. Final Detector-Block Design for Single-Plane Instrument:

The results of the design and experimental studies carried out in the first year of the project indicated that the 1mm resolution at the field center as dictated by sampling was not achieved due to performance limitations of the 12 crystal detector blocks. Further some loss of sensitivity due to this limited performance was observed in the prototype device. It was therefore decided to use slightly wider LSO crystals (1.2 mm) in the final design. Such wide crystals would limit the maximum resolution to the 1.2 mm achieved with the prototype but would improve the performance of the blocks considerably. Further, it was decided to increase the depth of the crystals from 5mm to 7 mm resulting in a factor of 2 improvement in sensitivity. Figure 2 shows a schematic diagram of the new detector block. Experimental studies to optimize the propagation of light within the blocks led to the surface preparations shown in the diagram. Figure 3 shows the ratio spectrum resulting from measurement of 511 keV photons from a uniform source. The end crystals are more clearly resolved than those in the prototype block. Also, the dynamic range between the center and edge crystals is lower than the corresponding range in the twelve-crystal block indicating better light collection at the block center. It is expected , based on these Improvements, that the energy discrimination needed to Identify the crystals in the 12 crystal block can be reduced resulting in a further increase in overall sensitivity.
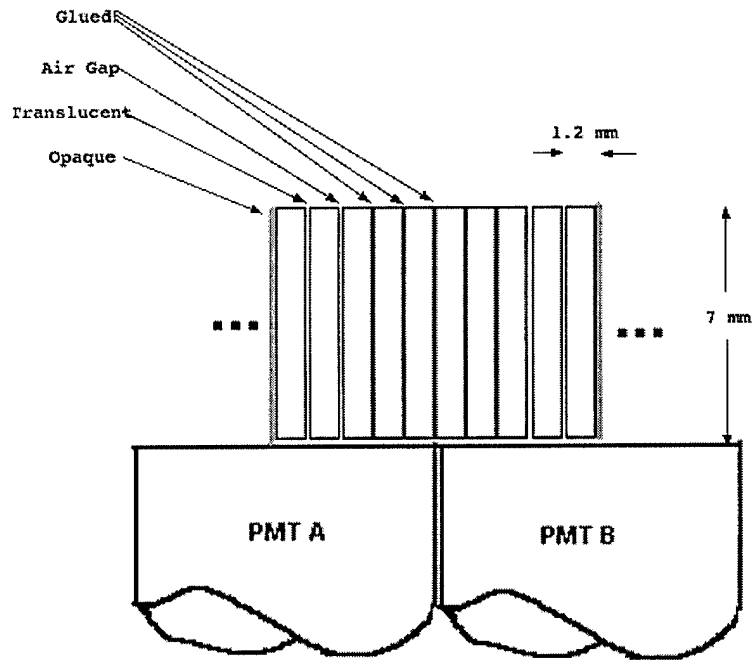
2D TEN-CRYSTAL LSO BLOCK DESIGN

Figure 2: Schematic of ten crystal LSO block showing surface treatments.

Ratio Spectrum - 10 Crystal LSO Block
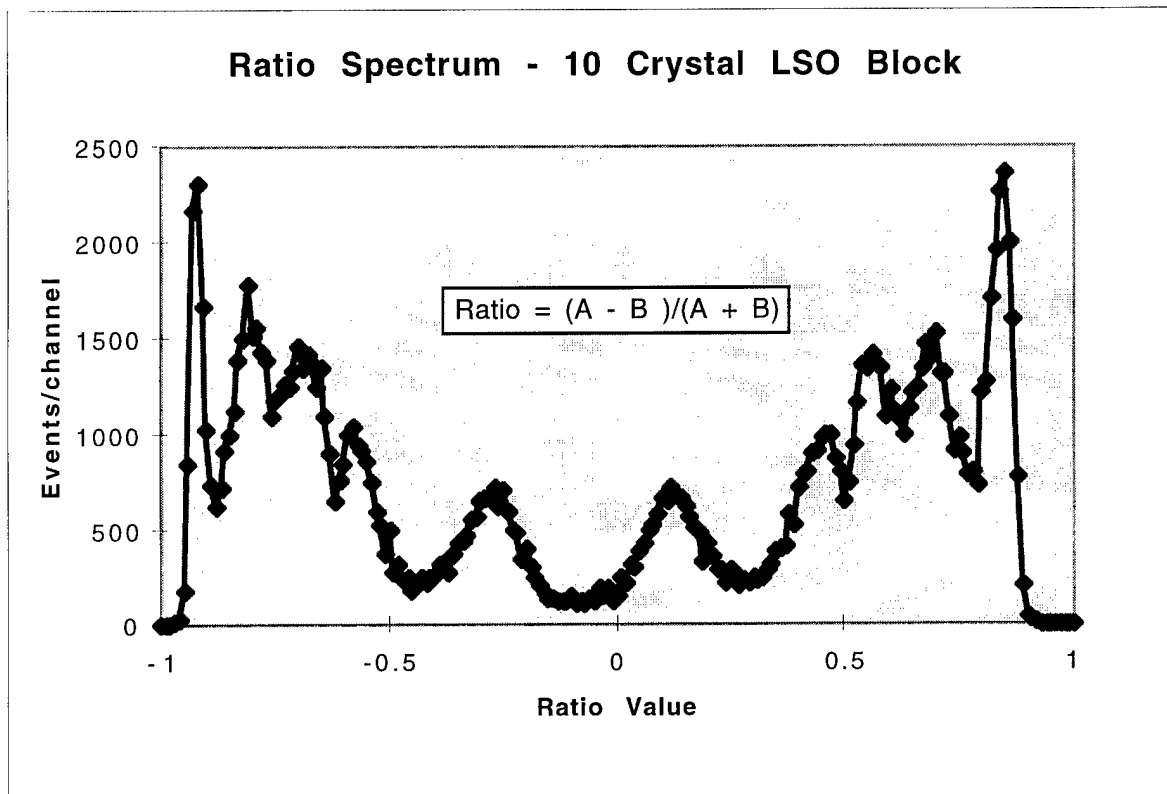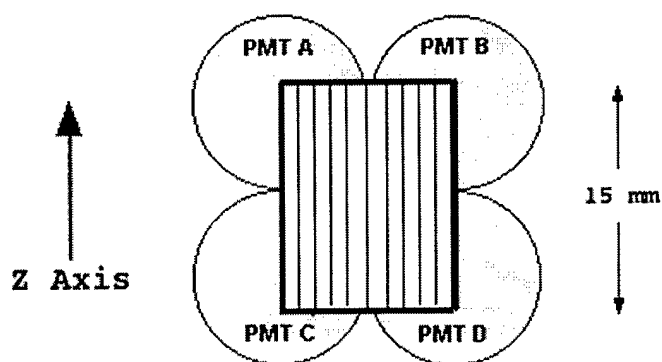

$$Ratio = (A - B)/(A + B)$$

Figure 3: Measured ratio Spectrum for ten-crystal block. The end crystals are more clearly resolved than those in the prototype block. Also, the dynamic range between the center and edge crystals is lower than the corresponding range in the twelve-crystal block indicating better light collection at the block center.

E. Detector Block Studies for Volumetric Instrument:

Although a single-plane (2-dimensional) instrument is useful in measuring long bones, it is limited to some extent by low sensitivity. An alternative way of stating this is that, in order to sample a large area of the bone, multiple images must be taken sequentially. As part of the development work associated with this project we have attempted to design a volumetric (3-dimensional or multi-planar) detector element which could form the basis of a future, higher sensitivity instrument. Most of the electronics and processing software developed in this project could be generalized easily for use with such an instrument. Several bench-top prototypes of volumetric detector elements have been studied and preliminary results from the most promising one are presented here. The basis of this design is that light collected and used to identify a given crystal within a block also contains information on the vertical (z) position of the interaction within the block. Thus, if the z thickness of the crystals is extended, it is possible not only to identify which crystal

10

gave rise to the interaction but where along the z dimension the interaction took place. The latter information can then be used to sort events into a set of transaxial planes, each one of which is equivalent to one data set collected by the single-plane instrument. Our preliminary results indicate that it is possible to separate at least five planes with 15 mm long (z) crystals. This alone would increase the system sensitivity by a factor of five. Further, using coincidence events between planes and volumetric reconstruction methods could result in as much as a factor of ten increase in sensitivity. A sketch of the prototype block is shown in figure 4. Preliminary experimental results for the performance of this block are shown in figures 5, 6 and 7.

3D TEN-CRYSTAL LSO BLOCK DESIGN

Figure 4: Schematic of ten-crystal volumetric block. The z-dimension is the direction of the plane thickness in the single-ring instrument

CRYSTALS: 7 mm deep, 1.2 mm wide, 15 mm high.
Surface Preparations Same as 2D-Block.

Transverse Ratio Spectrum - 3D Block

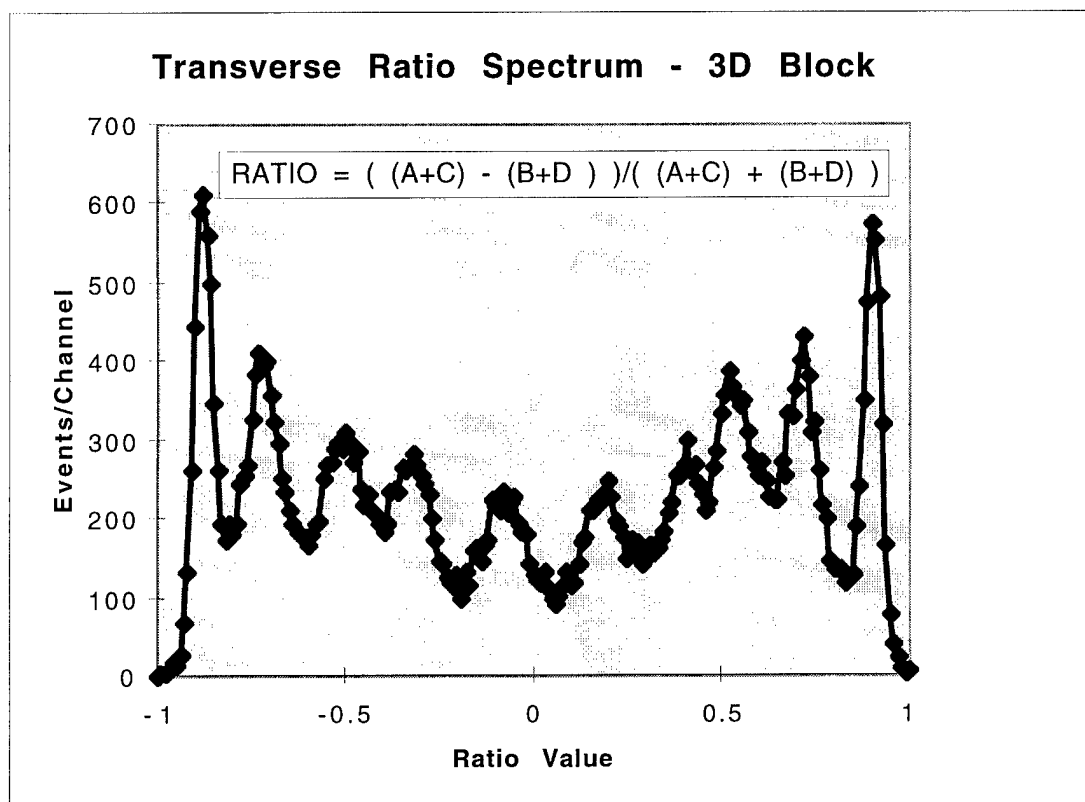$$\text{RATIO} = (\ (A+C) - (B+D) \ )/(\ (A+C) + (B+D) \ )$$

Figure 5: Transverse or in-plane ratio computed from phototube signals as indicated. The four PMT signals (A, B, C, D) are used as indicated to compute the ratio.

Axial Ratio Spectrum - 3D Block - Collimated Slit Source

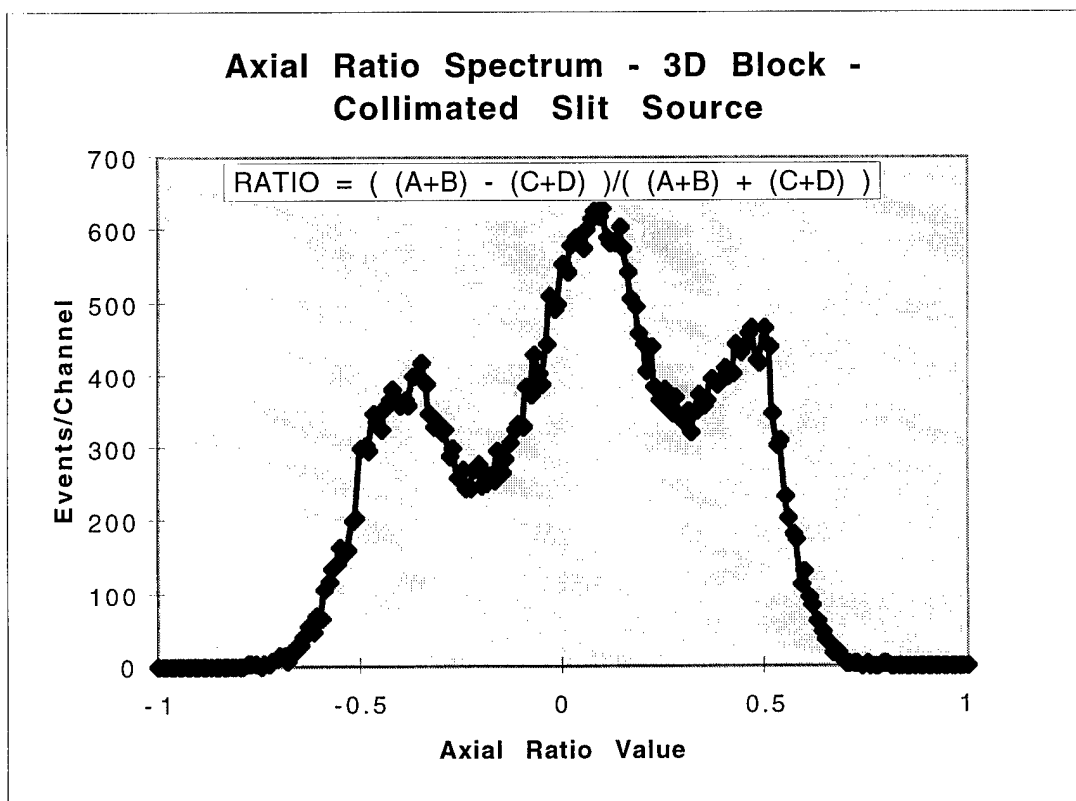$$RATIO = (\ (A+B) - (C+D)\ )/(\ (A+B) + (C+D)\ )$$

Figure 6: Axial ratio spectrum for a shielded line source of radioactivity placed near the 3D-block center. The z-axis ratio is computed from the four PMT signals (A,B,C,D) as indicated. The spectrum does not fill the full range of ratio values (-1 to 1) but is compressed due to background light in the crystals. This preliminary measurement indicates that there is sufficient information available to identify the z-coordinate.

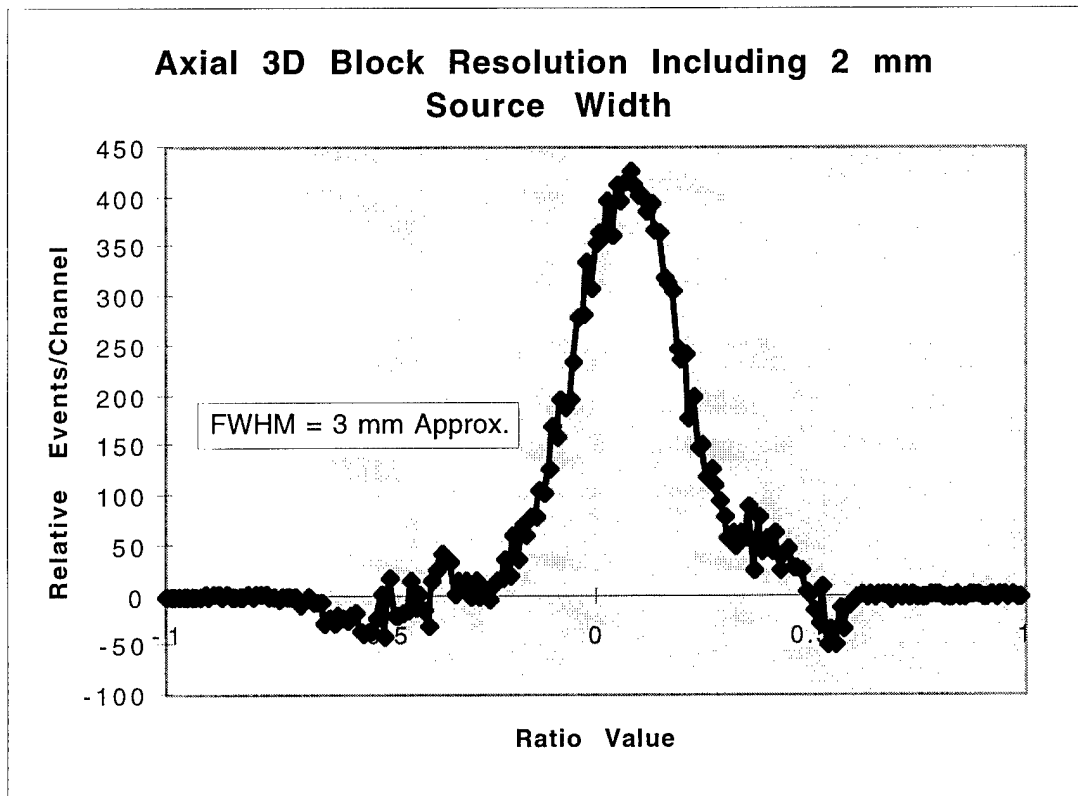**Axial 3D Block Resolution Including 2 mm Source Width**

FWHM = 3 mm Approx.

Figure 7: Preliminary estimate of the central z-axis resolution of the 3D block derived from the z-coordinate ratio spectrum by correcting for source width and background effects. A FWHM of 3 mm implies that the z-data could be binned into 5 planes over the 15 mm crystal extent.

F. - Electronic Design and Board Layouts:

Part of the goal in designing the instrument was to minimize the need for specialized electronics by making maximal use of software-based processing. Each PMT signal is processed by its preamplifier board to yield a timing pulse and an energy pulse. Leading-edge timing and delay-line shaping are used to identify coincident events. Coincidences are determined among twelve groups of three PMT signals. Once a coincidence is identified, all 36 PMT signals are digitized by the ADC boards and transferred as a group to the computer interface. Also, the total the total single event rate, which is used to generate a random coincidence correction, is transferred with each event.

The following circuit boards have been designed and are either completed or are currently being manufactured:

1. Preamplifier Boards - 36

2. ADC Boards   - 12
3. Coincidence Board   - 1
4. Interface Board   - 1

Cabling among the boards and computer is currently being
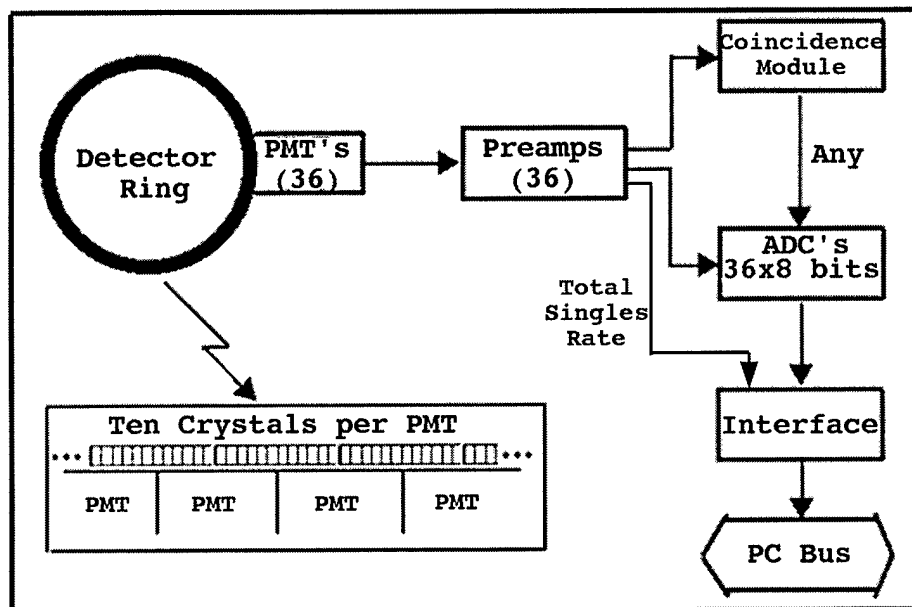assembled.

G. Data Acquisition and Software Development:

1. Data acquisition:

   One of the limitations of the prototype instrument is its inability to collect data at high countrates. To overcome this limitation a number of data acquisition hardware and software configurations were studied. To take advantage of the large body of development work which has been carried out in the PC-based data acquisition area, it was decided to commercially available acquisition hardware which uses the PCI Bus interface for the PC. The main requirements for the instrument under construction are high acquisition speed or data rate, ability to interface to the analog electronics and ability to buffer incoming data so that front-end processing can be carried out during acquisition. Test software was written for several commercially available boards as well as for an enhanced version of our current in-house developed acquisition board. The best commercial device evaluated was the PCIDIO-3240 board manufactured by Cyber Research . A modified version of our in-house designed interface was also evaluated on a 500 Mhz PC. It performed better than expected as illustrated in figure 9. Data collection modules have been written for both this interface and the PCIDIO-3240 interface so that either may be used with the instrument.
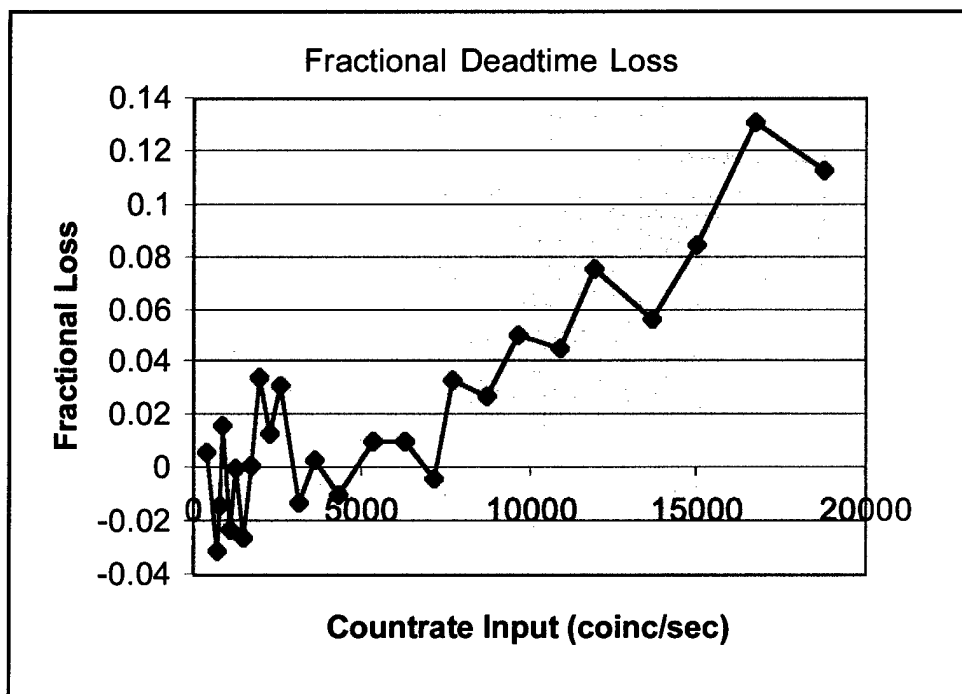

Figure 9: Measured count loss in computer interface due to deadtime. Data are for in-house constructed IF and a 500 Mhz Pentium Processor. The deadtime is less than 5% at 10k c/sec.

2. Image Manipulation and Display Software:

Two display packages have been made available for the imaging system. The first was written in-house using the MATLAB Graphical Interface Language. In the course of investigating display systems we discovered a public domain display program which was originally written at NIH but is now available (free) through a commercial supplier (Scion Image). This fully functional display package, originally written for use with autoradiographic data, has been adapted with minor changes. The features common to both programs include: grayscale and color display of both sinograms and reconstructed images: region-of-interest selection and extraction of data; profile extraction, image arithmetic and image processing (smoothing, etc.).

3. Software Development:

In order to collect, reconstruct and display PET data, a number of software modules are necessary. Our approach has been to develop software using C/C^{++} code in the Windows95/98 operating system. Software modules developed for the prototype system are in the process of being adapted and modified for use with the new system under Windows95/98. New features being added include: Graphical user interface, collection sequence editor, multiple frame collection with optional object motion, an automated sequential file naming routine and new file headers carrying complete information with each sinogram or image file. In addition implementation of corrections, scatter, deadtime, attenuation, uniformity and radioactive decay in the new software package is ongoing. Some of these corrections, uniformity and attenuation in particular, have been implemented in the prototype while the remaining ones are new to the final instrument.

4. Automatic Motion System:

In order to collect sequential images of long bones or small animals, it is necessary to have some method of moving objects reproducibly within the instrument's field-of-view. Ideally, the control of this device should be integrated with the camera control software for both ease of use and centralization of image information (i.e., storage of all image information in an image file header). To accomplish this we have adapted a commercially available motion controller and stepping motor (Advanced Microsystems). A software module to control this device and read position has been developed and is being integrated into the data acquisition program. In the final version of the software, an object's position relative to an initial reference

17

position can be specified and the object moved to that position before the start of each frame; the position being recorded with the frame data.. An option for user-specified (non-automated) positioning is also provided.

Initial experience with the device has demonstrated that positioning can be achieved and reproduced to +/- 0.25mm.

H. - Preliminary Animal Studies:

The physical performance characterization of the prototype instrument was completed at the beginning of this grant period. Most of the results were described in last year's report and will not be repeated here. They are summarized in a publication included in the appendix. A number of mouse imaging studies have been carried out in conjunction with another DOD-funded project at our institution (DAMD17-99-1-9555, A.L. Brownell, PI) which has approval for mouse studies with these instruments.

Figure 10 shows coronal sections of the brain of 25 gm mouse. Collection was begun 45 minutes after the injection of ^{18}F-fluorodeoxyglucose, a glucose metabolism tracer. Considerable detail can be seen including the olfactory bulbs in the first four images (top row) and well-separated cerebral cortex, temporal lobes and basal ganglia in the last three images (bottom row).

Figure 11 shows selected transverse images of glucose metabolism in the torso of a 25 gm mouse. structures visible include the kidneys (leftmost image) and bowel (center image).

Figure 12 shows a sequence of images in a 25 gm mouse after the injection of ^{18}F-Fluoride ion, a bone metabolism tracer. A great deal of detail can be seen in the skull (first three images row 1), the shoulders and upper extremities(last two images, top row), the chest (first three images, bottom row) and the pelvis (last two images, bottom row).

Figure 13 shows a sequence of images taken of the leg of a 2.5 kg rabbit starting below the knee. The tissue sample used (leg) was discarded after a biodistribution dissection study from another protocol (NIH Burn Trauma Center Grant 4P50GM21700-22).

Figure 14 shows one of our first attempts to image a monkey long bone (lower forearm) with ^{18}F-fluoride ion. A relatively low dose of 10mCi was injected. The radius and ulna are both visualized and the endostial and periostial surfaces are well separated and clearly seen. To-date we have done two of these preliminary studies in order to establish study parameters and injected dose.

These preliminary animal studies demonstrate the capabilities of the instrument and methodology developed to image small objects at very high (for PET) resolution. The bone studies in particular demonstrate that even in animals as small as mice, high quality bone kinetic studies can be carried out and that in larger animals, monkeys in particular, the periostial and end-ostial surfaces of the long bones can be resolved.

18F-FDG Mouse Brain Coronal Images
1.5 mm Spacing
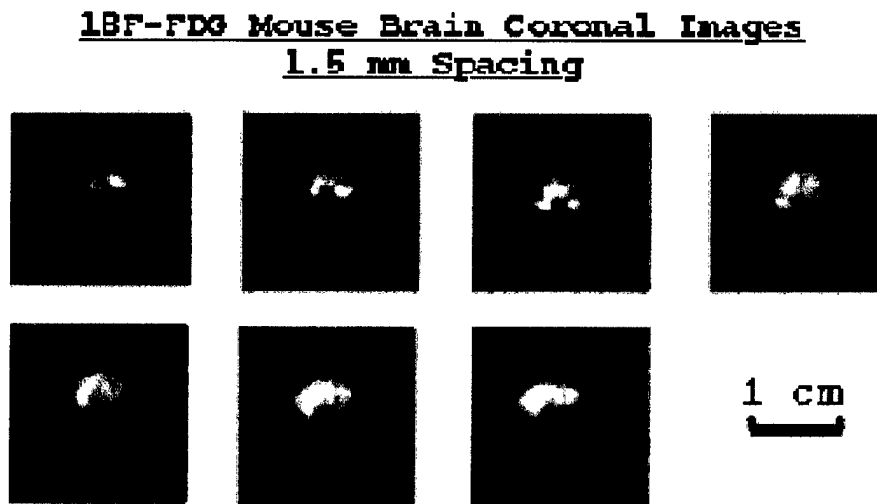

Figure 10: 18F-FDG Images of mouse brain started at 40 minutes after injection of 2 mCi of radioactivity. Each image was collected for approximately 20 minutes.

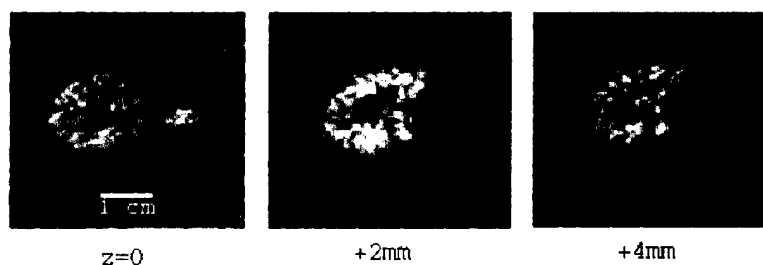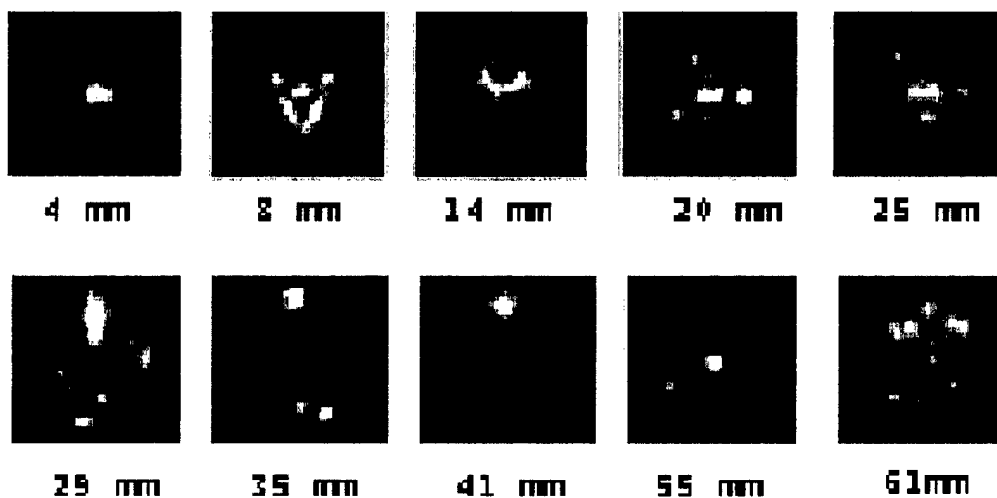## 18F-FDG Images in Mouse Lower Torso

z=0   +2mm   +4mm

Figure 11: Sequential images of the lower torso in a 25 gm mouse begun 40 minutes after the injection of 2.4 mCi of 18F FDG. The plane separation is 2 mm. Each image was collected for approximately 15 minutes.

18F-Fluoride Ion Mouse Images

4 mm   8 mm   14 mm   20 mm   25 mm

29 mm   35 mm   41 mm   55 mm   61mm

Approximately 0.25-0.5M events per Image

Figure 12: 18F Fluoride Images of mouse skeleton beginning after injection of 1 mCi of radioactivity. Each image was collected for approximately 10 min.
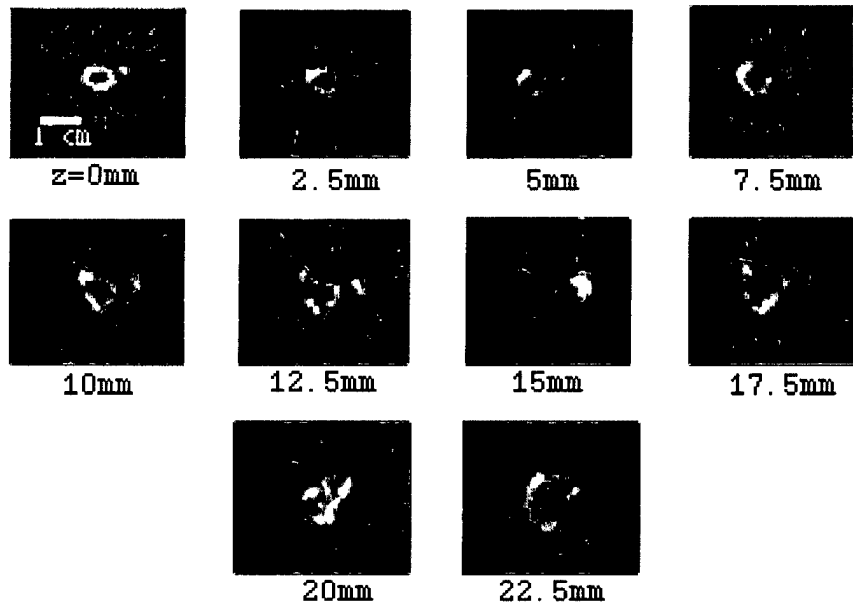
18F Sequential Images in Rabbit Leg

Figure 13: Sequential images, separated by 2.5 mm, of lower leg of a 2.5 kg rabbit begun twenty minutes after the injection of 15 mCi of 18-F Fluoride . The sequence moves up the leg toward the knee. Each image was collected for approximately 10 minutes. NOTE: this was a postmortem sample obtained after it was discarded from a biodistribution studied with separate animal approval (NIH Burn Trauma Center Grant # 5P50GM21700-22).
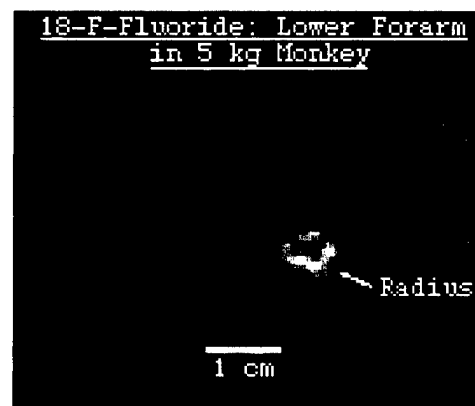

Figure 14: Image of lower forearm of 5 kg monkey begun 15 minutes after the injection of 20 mCi of 18-F-Fluoride. Approximately 20 minute imaging time. The periostial and endostial surfaces of radius and ulna are clearly seen.

21

IV. - KEY RESEARCH ACCOMPLISHMENTS:

1. Specification of Final Single-Plane Instrument.
2. Construction of Single-Plane Instrument Near Completion (expected completion: November, 2000).
3. Detector module for a multi-plane instrument designed and experimentally studied.
4. Preliminary animal studies undertaken and bone imaging of monkey extremities begun.

V. - REPORTABLE OUTCOMES:

A number of the studies carried out during this grant period are reportable in fact some have already been published. These include:

1. Physical characterization of 1 mm prototype device completed.
2. Second Generation single plane device designed and under construction.
3. Volumetric detector block designed and evaluated.
4. High resolution studies in small animals and monkey extremities begun. To our knowledge these are the highest resolution in-vivo PET studies anywhere to date.

VI. - CONCLUSIONS:

During the first year of the project we established a design for a high resolution PET instrument for bone imaging. The design was based on simulation studies of PET detector and system properties, benchtop experiments with detector elements and electronic circuit designs, and the construction and evaluation of a prototype imaging device as an experimental verification of feasibility. The main conclusion from this work was that it is feasible to carry out small-scale PET imaging at resolutions approaching 1mm. In the second (current) year of the project we applied the results of the first year to generate a final design for an instrument and to construct that instrument. Construction is almost complete (expected completion November, 2000). The construction of this instrument was the major project goal for the second year.

We have carried out preliminary imaging studies of monkey long bones during the latter part of this project period. We have done two studies to date. The main goal of these preliminary studies is to establish the imaging parameters for future monkey studies. This was also a major goal of the second year period.

As an outgrowth of our studies of detector module designs for this project, we have designed, constructed and begun preliminary testing of a 3-D (volumetric detector module which could form the basis of multi-planar high-resolution PET instrument which would image multiple planes simultaneously. Although not directly stated as a project goal, this development is intimately related to our long term goals of high resolution of bone kinetic measurements in monkeys and humans.

Very high resolution PET imaging is the only technique currently available which could be used for the bone growth studies in-vivo. Very high resolution PET imaging is likely to have application in many other areas as well. The most exciting, perhaps, is the measurement of various physiological and biochemical parameters in mice. Genetically-altered-mouse-based disease models are becoming widely used for the study of abnormal physiology and the very high resolution offered by the instruments developed in this project is ideal for imaging them.

VII. - APPENDIX:

Previously Reported:

1. "Development of a Small Animal Pet Imaging Device with Resolution Approaching 1mm", JA Correia, CA Burnham, D Kaufman, AJ Fischman, J Nucl Med 40:285P (1999) Abstr.

2. "Development of a Small Animal Pet Imaging Device with Resolution Approaching 1mm", JA Correia, CA Burnham, D Kaufman, AJ Fischman, IEEE Trans Nucl Sci 46:631-635 (1999).

3. "A Pet Imaging Instrument for High Resolution Rat and Mouse Imaging ", JA Correia, CA Burnham, D Kaufman, E. Carter, AL Brownell, AJ Fischman, "High Resolution Imaging in Small Animals with PET, MRI and other Modalities: Proceedings", pp 63-64, Amsterdam (1999).

New Since Last Report:

4. "Performance of a Small Animal Pet Imaging Device with Resolution Approaching 1mm", JA Correia, CA Burnham, D Kaufman, AJ Fischman, IEEE Nuclear Science Symposium and Medical Imaging Conference Record, M7:pp 1-5 (1999).

5. "Designs for Small Animal PET Systems" ,Abstr., JA Correia, CA Burnham, D Kaufman, AJ Fischman, Congress of European Assoc. Nuclear Med, (Sept, 2000).

6. Design Considerations for Small-Animal PET Devices with Resolution Approaching 1 mm", JA Correia, CA Burnham, D Kaufman, AJ Fischman, IEEE Trans Nucl Sci, Accepted(2000).

No. 1257

FULL FOV HOLE ANGULATION ERROR MAPPING OF PARALLEL HOLE COLLIMATORS USING A PRETILTED COLLIMATED FLOOD SOURCE.

A. J. Arends, M.J. A. de Voigt, A. van Lingen*, Medical Physics Department, Catharina Regional Hospital, Eindhoven, The Netherlands; Eindhoven University of Technology, Accelerator Laboratory, Eindhoven, The Netherlands; Department of Nuclear Medicine, Free University Hospital, Amsterdam, The Netherlands. (100351)

Objectives: Hole angulation errors (HAE) lead to misregistration of events. For SPECT limits as low as 0.25° have been proposed. QC-methods using point sources yield only local HAE-values, while mapping methods published require dedicated hardware/software. We propose a simple method for full FOV HAE mapping, requiring only standard NM-equipment. **Method**: For low energy photons collimators show almost purely geometric transmission (Tr). The concept used is the strong dependence of geometric Tr through a stack of two collimators on their alignment. The collimator to be tested (A) is mounted on the detector, and placed closely above a *collimated flood source* (parallel reference collimator **B**, preferably Hi-Res, on top of a ^{57}Co or ^{99m}Tc flood source). *Pretilting* maximizes sensitivity (dTr/dα)for small HAE-values and yields directional information. We apply a pretilt angle β that leaves Tr(β) at ≈50% of Tr(0°). Two high count transmission scans are performed at orthogonal pretilts. Areas with HAE will show up as cold or hot zones, depending on their magnitude and direction relative to the pretilt applied. If B is clinically used too, positive findings require an additional test (rotate B or use a point source) to decide whether A or B contains HAE. **Results**: Sensitivity and lower detection limit of the method depend on: type of collimators A and B, counts acquired, and uniformity of detector and flood source. Using two LEHR's (hexagon 1.5x38mm and 1.4x32.8mm) we found a dTr/dα of **20% per 0.25°** of HAE at β=1.9°. Four out of ten collimators showed unacceptable HAE during acceptance tests, and one at regular QC. **Conclusions**: The method proved to be valuable in acceptance tests and regular QC. It is sensitive and produces full FOV maps of HAE. Errors ≥0.25° are detectable and were observed in several collimators.

No. 1258

DEVELOPMENT OF A SMALL ANIMAL PET IMAGING DEVICE WITH RESOLUTION APPROACHING 1MM.

J. A. Correia*, C. A. Burnham, D. Kaufman, A. J. Fischman, Massachusetts General Hospital, Boston, MA. (500477)

Small animal imaging presents a situation where positron range effects and sampling are the dominant physical limitations to spatial resolution. Annihilation-pair non-colinearity and scatter are minimized due to the small dimensions of both instrument and subject. Theoretical and simulation studies support the idea that spatial resolution on the order of 1mm can be achieved with ^{18}F and ^{11}C. The availability of LSO as a scintillator material for PET makes possible the design of detector modules with resolution approaching one millimeter. The purpose of the work reported here was to design and construct a prototype single-plane, high resolution PET instrument using LSO detectors. The approach taken was to develop a simple prototype that maximizes the use of software data processing to minimize electronics construction. The detector array consists of a single ring of 360 1x4.5x5 mm LSO crystals organized into blocks of 12 crystals each viewed by two photomultipliers. To achieve high resolution, thin crystals (5 mm) are used for several reasons; first, the use of thin crystals moderates the degradation and non-uniformity of resolution caused by multiple detector penetration at photon incidence angles far from the normal, and secondly, blurring due to multiple interaction sites is reduced. The choice of thin crystals represents a sacrifice in sensitivity to preserve resolution. The system is also operated with a low energy threshold to maximize the number of single-interaction-site events. Crystals are identified using two block-specific lookup tables, one applied to the normalized pm tube differences and one applied to the total block energy. Reconstructed resolution was measured using 0.42 mm diameter 18F line sources. The resolution at the center of the field is 1.2 mm and the radial resolution at 2.5 cm radius is 1.65 mm. System sensitivity was measured using cylindrical water-bath sources of various diameters yielding 1.2 cps/uCi/cc for a 0.5 cm source and 72 cps/uCi/cc for a 4.5 cm source. Imaging studies in rats and mice with ^{18}F- FDG and several ^{11}C receptor compounds have been begun.

No. 1259

THE EVALUATION AND CALIBRATION OF FAN-BEAM COLLIMATORS.

J. L. Mahowald, P. D. Robins, M. K. O'Connor*, Mayo Clinic, Rochester, MN. (100046)

The aims of this study were a) to determine the true focal-length of a fan-beam collimator and b) to calibrate image size (mm/pixel) for each collimator to permit inter-comparison of image data acquired on different gamma camera systems. Methods: 6 fan-beam collimators were evaluated on 3 SPECT systems. Tomographic images of a line of Co-57 markers were obtained at 3 radii of rotation. From the transaxial images the distance between markers was measured in pixels and used to determine pixel size in mm / pixel. The system value for the focal length of the collimator was modified by up to + 100 mm and transaxial images were again reconstructed. SPECT images of a 3-D brain phantom were reconstructed using both the original and modified values of collimator focal length and thickness. Co-registration and subtraction of the reconstructed transaxial images was used to evaluate the effects of changes in collimator parameters. Results: Pixel size in the reconstructed image was found to be a function of both the radius of rotation and the focal length. At the correct focal length, pixel size was essentially independent of the radius of rotation. For all 6 collimators, true focal length differed from the original focal length by up to 26 mm. These differences in focal length resulted in up to 6% variation in pixel size between systems. Pixel size between the 3 systems was standardized by altering the value for collimator thickness. Subtraction of the co-registered SPECT images of the 3-D brain phantom was significantly improved after optimization of collimator parameters, with a 35-50% reduction in the standard deviation of residual counts in the subtraction images. Conclusion: Accurate knowledge of the focal length of a fan-beam collimator is an important parameter on multi-detector systems for optimum image quality and where accurate image co-registration is required.

No. 1260

EFFECT AND CORRECTION OF DETECTOR SAG IN SPECT SYSTEMS.

J. Peter*, D. R. Gilland, J. E. Bowsher, M. P. Tornai, R. J. Jaszczak, Duke University Medical Center, Durham, NC. (101118)

Objective: Large field-of-view SPECT detectors mounted to one side of the gantry ring may deflect, or sag, due to gravity. The goal of this study was to investigate the effect of detector sag on SPECT image quality. *Methods*: Monte Carlo simulations were performed for several SPECT geometries over a range of displacement magnitudes using analytical point source phantoms. Phantom data were reconstructed using FBP and OSEM. A fixed detector mounting point is located at the center of the gantry-side detector surface. As the detector rotates over 2π, angular displacement of the collimator plane is rotational about the mounting point in azimuthal direction, θ, in the collimator plane and in polar direction, φ, out of the collimator plane. The magnitude of displacement varies with projection angle α whereby θ(α) and φ(α) follow the same functional relationship but are shifted by $\pi/2$, i.e. extremal azimuthal displacement corresponds to zero polar displacement and visa versa. *Results*: The detector rotational displacement results in a non-uniform displacement map of points on the collimator surface; points further away from the mounting point have a longer displacement vector. Angular displacement artifacts are clearly identifiable in projection data sinograms: azimuthal detector sag leads to out-of-plane artifacts; polar displacement results in center-of-rotation artifacts. For a parallel beam detector with radius 40cm and maximum angular detector sag of 1.5deg, 1cm displacement artifacts and substantial shape distortions in the reconstructed image are visible. *Conclusion*: Slight detector sagging can introduce significant image artifacts. These results indicate the importance of minimizing sag when designing scanners. Also, detector sag could be modeled within iterative reconstruction algorithms, which can account for physical detector characteristics.

Poster Sessions

Development of a Small Animal PET Imaging Device with Resolution Approaching 1mm

J.A. Correia, C.A. Burnham, *Senior Member IEEE,* D. Kaufman, A.J. Fischman

Massachusetts General Hospital, and Harvard Medical School, Boston, MA 02114

Abstract

The work presented here describes progress in the design and construction of a single-plane PET tomograph having spatial resolution approaching 1 mm. The system consists of a 12 cm diameter ring with 360 LSO detectors viewed by 30 photo-multiplier tubes. Thin (5 mm) crystals and a low energy threshold are used. Crystals are identified using both position arithmetic and energy criteria. To-date the system construction has been completed, system tuning carried out and imaging studies begun.

I. INTRODUCTION

Positron emission tomography (PET) has achieved major successes during the past ten years as a metabolic imaging modality, especially in human and large animal subjects. Instrumentation for use in these regimes has become highly developed and reliable and is used routinely in many laboratories throughout the world. Recently, a number of workers have designed and successfully constructed instruments which image at higher resolution over small-scale fields, with the goal of imaging small animals such as monkeys, rats and mice [1-11].

Small animal imaging presents a situation where positron range effects and sampling are the dominant physical limitations. Annihilation-pair non-co-linearity and photon scatter are minimized due to the small dimensions of both instrument and subject. Theoretical and simulation studies support the idea that spatial resolution on the order of 1mm can be achieved with ^{18}F and ^{11}C [12-14]. The availability of LSO as a scintillator material for PET leads to several possible approaches to designing detector modules for PET systems having spatial resolution approaching one millimeter [15].

The purpose of the work reported here was to assess the feasibility of 1mm imaging by designing and constructing a prototype high resolution PET instrument using LSO detectors. The approach taken was to design and construct a simple prototype with as much flexibility as possible in hardware and software implementation. A simple design allows for straightforward modification and adaptation.

II. SYSTEM DESIGN

A. *General Design*

Simulation studies of the geometry including positron range, annihilation non-co-linearity and scatter have been used to develop the design presented here. The approach maximizes the use of software data processing to minimize electronics construction and maintain flexibility. A system block diagram is shown in figure 1.
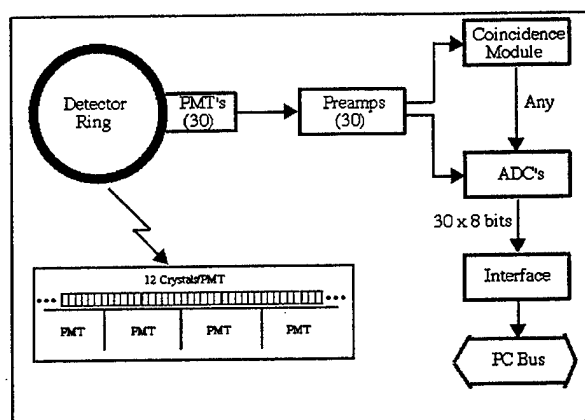

Figure 1: System Block Diagram

The detector array consists of a single ring of 360 1x4.5x5 mm LSO crystals organized into blocks of 12 crystals each viewed by two RCA 647 photomultipliers (PMT's) in a one dimensional implementation of the geometry proposed by Wong [16]. To achieve high resolution, thin crystals (0.5 cm) are used for several reasons; first, the use of thin crystals moderates the degradation and non-uniformity of resolution caused by multiple detector penetration at photon incidence angles far from the normal, and secondly, blurring due to multiple interaction sites is reduced [14]. The choice of thin crystals represents a sacrifice in sensitivity to preserve resolution.

The PM Tube signals are processed for timing and position. The coincidence logic uses the timing signal to identify any coincidence event from the central volume of the detector. The coincidence resolving time of the circuitry is 16 ns. The 30 linear position signals are DC coupled to the sample-and-hold ADC. Pulse shaping equivalent to single

delay line clipping is used. When a coincidence event is detected the 30 signals are simultaneously sampled and converted to thirty 8 bit words. The use of an 8 bit ADC is a compromise between speed and accuracy. The deadtime is limited by the time required to transfer, process and store an event in the computer. The sample update pulse interval is varied to minimize this deadtime. The preamplifiers, coincidence circuits and digital conversion circuits were implemented using standard logic elements. Provision has been made for direct and indirect estimation of random coincidences by measurement of triple coincidence and delayed coincidences.
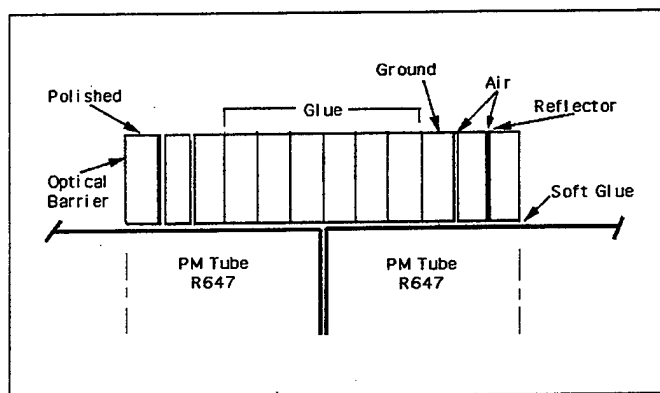

Signal vs Position Average Block Response

Figure 3: Measured relative crystal signal. Average over 30 blocks.

Figure 2. Detail of Block Design showing the various surface preparations used.

Ratio Spectrum - Typical Block
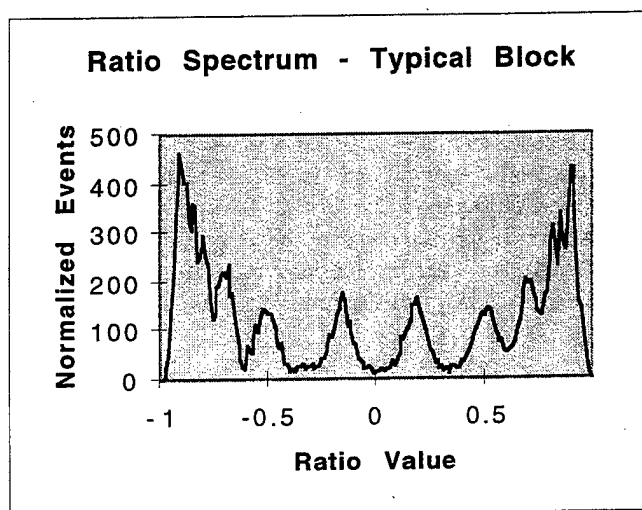
Figure 4.: Ratio from typical block measured with ⁶⁸Ge. Photofraction events.

B. *Block Design*

The individual blocks were designed based on a combination of computer simulations and experimental measurements of the optics for various geometries. The eight interior crystal faces are glued together in a jig with an 8° taper in order to point them toward the ring center. The next two on each side are separated from central crystals and each other by an air gap. The two outside crystals have polished surfaces and a partial reflector isolates them from the adjacent crystals. A reflector is used between blocks. The average fractional signal from each of the crystals for 0.511 keV photons is shown in figure 3. Approximately 1/3 of the light from the peak signals is lost and the energy resolution of the blocks at 0.511 keV is 17% at the center.
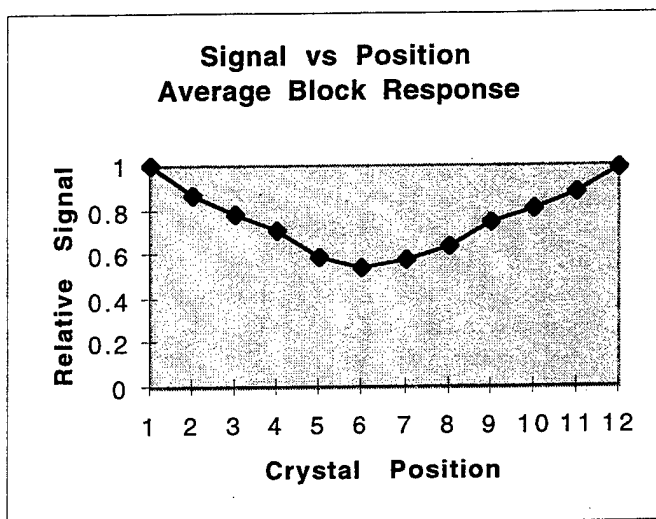
C. *Signal Processing*

When a coincidence event is registered by the hardware, the 30 PMT signals are transferred to the computer. The sum of neighboring pairs of PMT signals is computed and if a sum exceeds both neighboring sums and an energy threshold, a block is identified. If three blocks are identified, a triple coincidence is recorded. When exactly two blocks are identified within a data set the processing proceeds to the identification of the individual crystals within each.

The normalized difference (R) of PMT signals (A and B) in each block is determined as follows:

$$R = (A - kB) / (A + kB) \qquad (1)$$

and if an energy criterion to select only photopeak events:

$$E > E_{threshold} \quad \text{and} \quad E_{lower} < E < E_{upper} \qquad (2)$$

is met, a particular crystal is identified, otherwise the event is rejected.

A plot of the **R** spectrum from a typical block is shown in figure 4. Figure 5 shows the average bounds for the 30 blocks and figure 6 the individual-crystal energy spectra from a typical block.
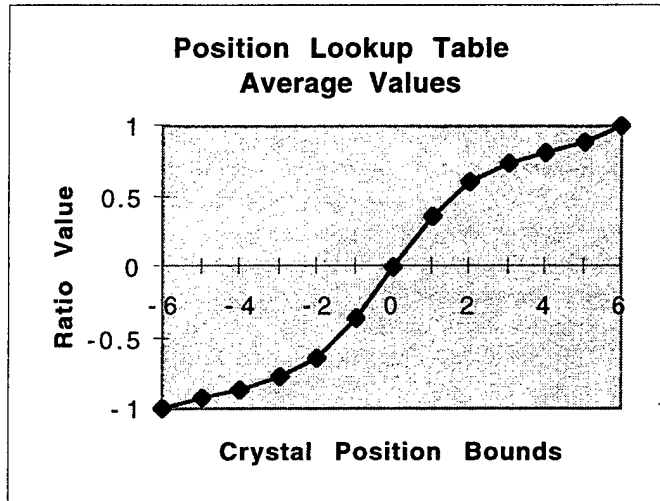

Figure 5: Measured ratios averaged over 30 blocks plotted as a function of ratio with crystal bounds indicated.
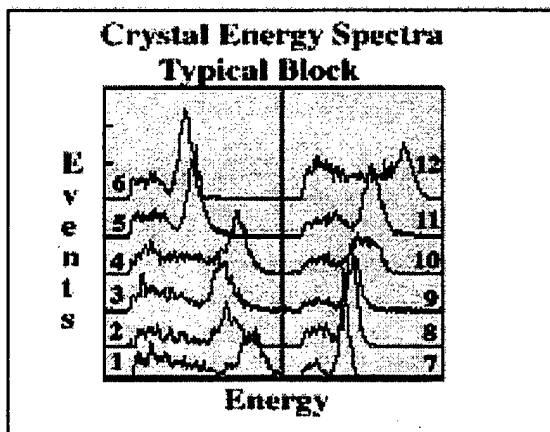

Figure 6: Energy spectra measured from a typical block using a ^{68}Ge source.

The PMT gains are adjusted such that the maximum signal of each utilizes the full dynamic range of the ADC. A

gain correction (**k** in equation 1), implemented via a lookup table, is then applied in the **R** calculation to force the ratio at the center of each block to zero.

A given value of **R** is associated with an individual crystal within the block via a lookup table specifying the lower and upper levels of the ratio values for that crystal. A good event is recorded if the boundary conditions are met and the phototube-sum, or total energy, signal is within a window derived from the crystal energy spectra. Boundary and energy lookup tables are specified for each block to account for small variations in crystal properties and alignment. The determination of the lookup tables is an iterative process in which a starting set of boundaries are specified from **R** plots taken with wide energy windows, then a set of narrower energy windows are specified from the energy spectra and the process repeated until an optimum is reached.

Coincidence data are mapped to a sinogram format for storage, corrected for sensitivity, randoms and attenuation and reconstructed using a standard convolution-backprojection algorithm.

III. SYSTEM PERFORMANCE

Reconstructed resolution was measured using 0.42 mm diameter ^{18}F line sources (22 gauge needles). Reconstructions were done with a ramp filter having a cutoff frequency of 2 mm^{-1}. Figure 7 shows an example of these measurements and table 1 summarizes the results. The resolution at the center of the field is 1.25 mm and the radial resolution at 2.5 cm radius is 1.75 mm.
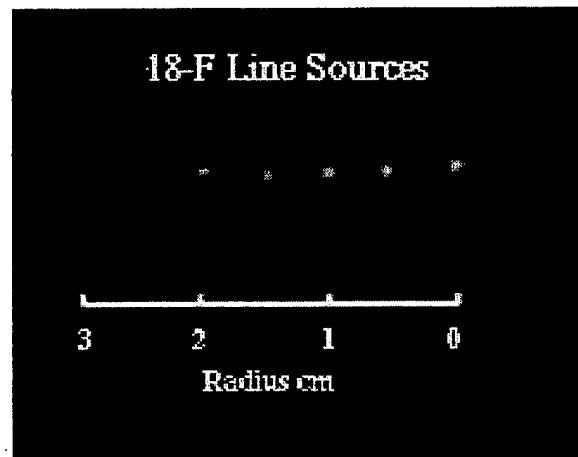

Figure 7: Reconstructed Image of six 0.4mm 18F line sources 0.5 cm apart. The scale shown is at 1 cm intervals with the field center at the right.

The axial resolution of the system at the center of the field was measured using a point source of ^{18}F stepped through the field in 0.1 mm steps. The axial resolution determined by this method was 1.8 mm for the results presented here. In general the axial resolution can be varied by adjusting the distance between two Pb collimator sections shielding the detectors. These collimators consist of two annuli of 5 cm inner radius and 12 cm outer radius. Each annulus is 6 cm long in the axial direction. In addition, the detector ring is shielded on both sides by a 1.25 cm annular Pb plate.

Table 1: Spatial Resolution at Various Field Radii Measured with 0.42 mm Diameter Line Sources.

| RADIUS (cm)	FWHM (mm)	FWTM (mm)
0	1.25	2.45
0.5	1.23	2.50
1.0	1.30	2.60
1.5	1.35	2.60
2.0	1.61	3.0
2.5	1.72	3.0

System sensitivity was measured with a centrally located point source of ^{18}F, a ^{68}Ge pin source and uniform fields of various diameters containing ^{18}F. Each uniform field source was approximately 4 cm in z-extent. The results of these measurements are summarized in table 2. The sensitivity listed represents all true coincidences formed by events above a 150 keV energy threshold.

Table 2: Measured sensitivity for cylindrical objects of varying diameter. The reported sensitivity includes all events above 150 keV. The point source sensitivity was measured with an ^{18}F point and is given in units of cps/uCi.

Diameter (cm)	Sensitivity (cps/uCi/cc)
0.5	3
2.0	40
2.5	69
3.5	145
4.5	204
Point	30 cps/uCi

Preliminary studies in rats have been begun as a means of testing the performance of the instrument under actual laboratory conditions. To-date, only imaging studies at low countrates have been carried out. Figure 8 shows three coronal images of a rat brain after injection of 4 mCi of ^{18}F-FDG. The collection time for each image data set was approximately twenty five minutes.

Figure 8: Coronal slices, 1.8 mm thick, in rat brain after injection of 4 mCi ^{18}F-FDG. A: 1 M events. Location: 15 mm forward of inter-aural line. High-uptake structures are the tips of the olfactory bulbs. B: 2.5 M events. Location: 10 mm forward of inter-aural line showing cerebral cortex and striatum. C: 1.0 M events. Coronal image of the posterior of the brain.
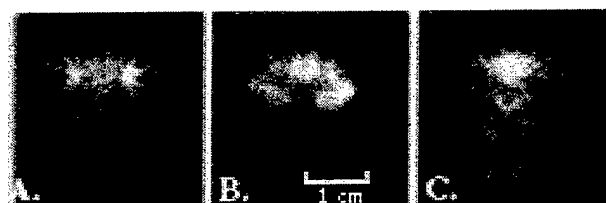
IV. CONCLUSIONS

The possibility of PET imaging with LSO detectors at resolution approaching 1 mm has been demonstrated in a prototype single-plane instrument. Resolution degradation is moderated by the use of thin crystals to the degree that objects up to approximately 3.5 cm diameter show only minimal degradation and objects up to approximately 5 cm in diameter maintain off-center resolution below 2 mm. The sensitivity of the instrument described here is low due to two factors. The first is the use of thin detectors for the reasons stated above and the second is the need to limit events in a given crystal to a range of energies about the photopeak due to poor light collection from the center of the blocks. This process reduces the efficiency for useful events by 40-60% depending on the energy window-widths chosen.

The measurements of spatial resolution using 0.45 mm diameter needles did not yield 1 mm resolution as at the center of the field as dictated by sampling. This is due in part to poor spatial resolution at the ends of some blocks. This loss of resolution accounts for the fact that the measured resolution is uniform over the central region of the field.

The wide range of signal amplitudes led to poor timing and sensitivity at the centers of some blocks. This effect has not been addressed to-date. Nevertheless the instrument may be effectively used for static imaging situations such as FDG imaging with moderate injected doses and may be useable, with larger injected doses, for some receptor studies. Preliminary tests of the instrument have been carried out in rat brain. The most effective use of this instrument in the future however is expected to be in imaging mice.

Ongoing work includes characterization and refinement of the detector-block design, crystal identification and time discriminator logic. Refinements of corrections for other physical effects such as field non-uniformity, attenuation, scatter and randoms in the projection data are also being

developed. A multiple ring version of this instrument with somewhat larger detector-ring diameter is currently being designed.

V. ACKNOWLEDGMENT

VI. REFERENCES

[1] Del Guerra A, Scandola M and Zavattini G, "YAP-PET: First Results of Small Animal Positron Emission Tomograph Based on YAP:CE Finger Crystals." *IEEE Transactions on Nocl. Sci.,* 45:3105-3108, 1998.

[2] Pichler B, Boning G, Lorenz E, et. al., "Studies with a Prototype High Resolution PET Scanner Based on LSO-APD Modules", *IEEE Transactions on Nucl. Sci.* 45: 1298-1302, 1998.

[3] Cherry SR, Shao Y, Silverman RW, et. al. , "Micropet: a high resolution PET Scanner for Imaging Small Animals, *IEEE Transactions on Nucl. Sci.,* 44:1161-1166, 1997.

[4] Weber S, Terstegge A, Engels R, et al, The KFA TierPET: Performance characteristics and measurements." *IEEE Nuclear Science Symposium & Medical Imaging Conference Record,* 1117-1120, 1997.

[5] Watanabe M, Okada H, Shimaza K, et. al., A high resolution animal PET scanner using compact PS-PMT detectors, *IEEE Transactions on Nucl. Sci.* 44: 1277-1282, 1997.

[6] Bruynodonckx P,Xuan l, Tavernier S, Zhang S, "Perforemance of a small animal PET scanner based on photosensitive wire chambers, *"IEEE Nuclear Science Symposium & Medical Imaging Conference Record,* 11335-1340, 1997.

[7] Moses WW, Virador SE, Derenzo SE, et al, "Design of a High-Resolution, High-Sensitivity PET Camera for Human Brains and Small Animals." *IEEE Transactions on Nucl. Sci.,* 44:1487-1491, 1997.

[8] Lecompte R, Cardorette J, Rodrique S, et. al."Initial Results from the Sherbrooke Avalanche Photodiode Positron tomograph", *IEEE Transactions on Nucl. Sci.* 43:1952-1957, 1996.

[9] Bloomfield PM, Rajeswaran S, Spinks T,et. al., "The design and Physical Characteristics of a Small-Animal Positron Emission Tomograph", *Physics in Med. and Biol.,* 40:1105-1196, 1995.

[10] Seidel J, Gandler WR, Green MV, "A Very High Resolution Single Slice Small Animal PET Scanner Based on direct Detection of Coincidence Line Endpoints", *Journal of Nucl. Med.* 35:p 40P, 1994.

[11] Tavernier S, Bruyndonckx P and Zhang S, "A fully 3D small PET scanner.", *Phys. Med. Biol.,* 37: 635-643, 1992.

[12] Correia JA, Burnham CA , Kaufman D, et. al, "Small Animal PET imaging Device - Preliminary Design Study", *J. Nucl. Med.* 38:44P, 1997

[13] Burnham CA., Elliott JT., Kaufman D., Chesler DA., Correia JA and Brownell G.L, "Single Interaction PET Detectors.' *IEEE Transactions on Nucl Sci,* 37:832-835, 1990.

[14] Burnham C A, Kaufman D E, Chesler D A, Stearns C W, Correia J A, Brownell G L: "A low-Z PET detector", *IEEE Transactions on Nucl Sci .* 37:832-834, 1990.

[15] Melcher C.L. and Schweitzer J.S, "Cerium doped lutetium oxyorthosilicate: A fast, efficient new scintillator." *IEEE Transactions on Nucl. Sci. ,* 39:502-505, 1992.

[16] Wong WH, Uribe J, Hicks K, et al, "A 2-dimensional detector decoding study om BGO arrays with quadrant sharing photomultipliers." *IEEE Transactions on Nucl. Sci.* NS41: 1453-1457, 1994.

A PET Imaging Instrument for High Resolution Rat and Mouse Imaging

J.A. Correia, C.A. Burnham, D. Kaufman, E. Carter, A. Brownell and A.J. Fischman
Massachusetts General Hospital, and Harvard Medical School, Boston, MA 02114

The current frontier in PET instrumentation lies at devices which image at higher resolution over small-scale fields, with the goal of imaging small animals such as monkeys, rats and mice. Small animal imaging presents a situation where positron range effects and sampling are the dominant physical limitations. Annihilation-pair non-colinearity and photon scatter are minimized due to the small dimensions of both instrument and subject. The availability of LSO as a scintillator material for PET leads to several possible approaches to designing detector modules for PET systems having high spatial resolution. The purpose of the work reported here was to design, construct and apply a prototype PET instrument with resolution approaching 1mm using LSO detectors. The approach taken was to design and construct a simple single-plane instrument with as much flexibility as possible in hardware and software implementation. A simple design allows for straightforward modification and adaptation.

The detector array consists of a single ring of 360 1x4.5x5 mm LSO crystals organized into blocks of 12 crystals each viewed by two photomultipliers. Each phototube views two blocks. Thin crystals (0.5 cm) are used to moderate the degradation and non-uniformity of resolution caused by multiple detector penetration at photon incidence angles far from the normal, and minimize blurring due to multiple interaction sites. The choice of thin crystals represents a sacrifice in sensitivity to preserve resolution. The PM Tube signals are processed for timing and position. The coincidence logic uses the timing signal to identify any coincidence event from the central volume of the detector. The 30 linear position signals are DC coupled to the sample-and-hold ADC. Pulse shaping equivalent to a single delay line clipping is used. When a coincidence event is detected the 30 signals are simultaneously sampled and converted to thirty 8 bit words. The deadtime is limited by the time required to transfer, process and store an event in the PC. The preamplifiers, coincidence circuits and digital conversion circuits were implemented using standard logic elements.

The individual blocks were designed based a combination of computer simulations and experimental measurements of the optics for various geometries. The eight interior crystal faces are glued together in a jig with an 8o taper in order to point them toward the ring center. The next two on each side are separated from central crystals and each other by an air gap. The two outside crystals have polished surfaces and a partial reflector isolates them from the adjacent crystals. A reflector is used between blocks. Approximately 1/3 of the light from the peak signals is lost and the energy resolution of the blocks at 0.511 keV is 17%.

Individual crystals are identified using three look-up tables customized for each block. These tables determine if the value of the normalized phototube difference and the energy of the event fall within defined ranges. The third table specifies a normalization factor to adjust for phototube gain differences.

The in plane spatial resolution of the device has been measured to be 1.2 mm at the field center, 1.27 mm at 1 cm radius and and 1.55 mm at 2 cm radius using 0.4 mm diameter line sources of 18-F. The axial resolution is variable but has been operated to date at 1.8 mm. The point source sensitivity for a source at the field center has been measured to be 30 coincidences/sec/μCi using an 18-F point source.The instrument has been applied to the imaging of adult rat brain, juvenile rat torso and adult mouse brain and torso using 18F FDG and fluoride ion as well as several 11-C labeled neuro receptor compounds.

The possibility of PET imaging with LSO detectors at resolution approaching 1 mm has been demonstrated in a prototype single-plane instrument. Resolution degradation is moderated by the use of thin crystals to the degree that objects up to approximately 3.5 cm diameter show only minimal degradation and objects up to approximately 5 cm in diameter maintain off-center resolution below 2 mm. The sensitivity of the instrument is low due to the use of thin detectors to preserve resolution and the need to limit events in a given crystal to a range of energies about the photopeak due to poor light collection from the center of the blocks. This process reduces the efficiency for useful events by 30-60% depending on the energy window-widths chosen.

The most effective use of this instrument in the future is expected to be in imaging mice. Future plans include the characterization and refinement of the detector-block design, further characterization of crystal identification and time discriminator logic, corrections for other physical effects such attenuation, scatter and randoms in the projection data and design of a multiplane device.

HIGH RESOLUTION IMAGING IN SMALL ANIMALS WITH PET, MR AND OTHER MODALITIES

Instruments and Applications in Modern Biomedical Research
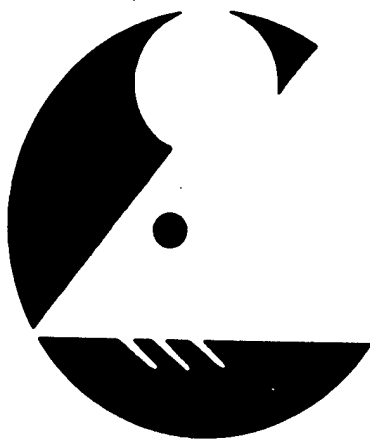
PROGRAM-ABSTRACTS

SEPTEMBER 27-29, 1999

ACADEMISCH ZIEKENHUIS VRIJE UNIVERSITEIT

AMSTERDAM, THE NETHERLANDS

Performance of Small Animal PET Instrument with 1mm Resolution

J.A. Correia, C.A. Burnham, D.E. Kaufman and A.J. Fischman

Massachusetts General Hospital, and Harvard Medical School, Boston, MA

Abstract

A single-plane PET imaging instrument using LSO detectors has been constructed to demonstrate the feasibility of imaging at 1 mm spatial resolution. The performance of this instrument has been evaluated in phantoms and small animals. Measurements presented include spatial resolution, sensitivity, countrate performance, linearity and field uniformity. Examples of several mouse imaging studies are also presented.

I. INTRODUCTION

The purpose of the work reported here was to evaluate the performance of a single-plane prototype small-animal PET instrument developed at our laboratory. The rationale for developing this prototype was to demonstrate the feasibility of imaging small-scale objects, particularly mice, at 1 mm spatial resolution and further to gain knowledge which will be applied to a second-generation design. The evaluation presented here consisted of measurements of a number of the instrument's physical properties as well as applications to physiological imaging in mice.

II. SYSTEM DESCRIPTION

The PET imaging system has been described in detail elsewhere [1-2] and therefore, only a brief description will be given here.

The detector array consists of a single ring of 360 1 x 1.5 x 5mm LSO crystals [3] organized into 30 blocks of 12, each block being viewed by two photomultipliers (PMT's) in a one-dimensional implementation of the geometry proposed by Wong [4]. The detector-element size limits the spatial resolution. A detector radial dimension of 5mm was chosen to moderate the degradation and non-uniformity of resolution caused by multiple detector penetration at photon incidence angles far from the normal, and to reduce blurring due to multiple interaction sites [5]. This choice represents a sacrifice in sensitivity to preserve resolution.

The crystal interfaces within each block have different treatments to optimize the amount of light reaching the two phototubes. Typically, the light collected at the block center is approximately 1/3 that at the block edge. Outputs of the thirty PM tubes are processed for timing and amplitude signals. The average crystal energy resolution is 17% at the block center for 0.511 MeV photons.

The coincidence logic uses the timing signal to identify coincidence events from the central volume of the detector with a resolving time of 16ns. Identification of a coincidence event results in the simultaneous sampling and digitization of all the linear PMT signals and their transfer to a PC for processing.

The software identifies a block when the sum of adjacent PMT signals is greater than its neighbors. The normalized difference (ratio) of PMT signals in each identified block is determined. If energy criteria are met, a particular crystal is identified, otherwise the event is rejected. Ratio-boundary and energy lookup tables are specified for each block to account for small variations in crystal properties. Coincidence data are mapped to a sinogram format for storage and subsequently corrected for sensitivity, randoms and attenuation and reconstructed using a standard convolution-back-projection algorithm.
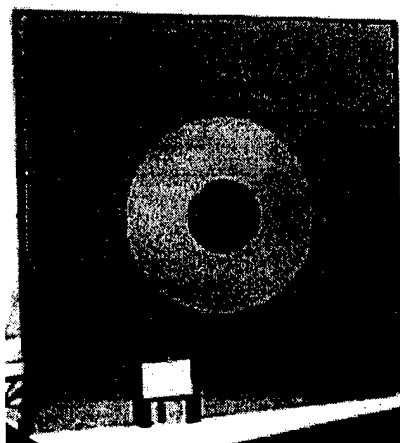

Figure 1: Photograph of PET Imaging System. A 3.5" computer disk is shown for scale.

III. SYSTEM PERFORMANCE

A number of physical performance measurements have been carried out in order to characterize the instrument's performance. These include both physical studies and preliminary imaging studies in mice. Summaries and specific examples are given in figures 2-11 and the text below. Studies were performed using a large-bore annular Pb collimator having an inside diameter of 7.5cm and a slice gap of 4mm.

The system in-plane spatial resolution was measured using 0.45 mm diameter line sources of ^{18}F placed at various distances form the center of the imaging field. The sources were filled with low levels of radioactivity to minimize countrates and therefore random coincidences. Images were reconstructed by filtered back-projection using a ramp filter. FWHM and FWTM were measured from profile plots through the reconstructed sources. These measured resolutions were corrected for finite source size by deconvolving the source response function. The results are shown in figure 2a. The resolution at the center of the field is 1.17mm and is 1.66mm at 2.5cm radius. An alternative measurement of the resolution is shown in figure 2b. 1cm x 1cm x 0.75cm-thick polyethylene blocks, each having an array of wells of varying size and spacing, were filled with ^{18}F solution and imaged. The smallest array, 1.25mm holes at 2.5mm separation is clearly visualized.

The axial resolution at the center of the field was measured by moving a point source of ^{18}F through the field in 0.1mm steps. The result was 1.75mm FWHM and 3.3mm FWTM as indicated in figure 3

Figure 2b: Spatial resolution phantom consisting of 1 x 1 x 0.75cm polyethylene blocks containing arrays of ^{18}F-filled wells. The well diameters and spacings are indicated.
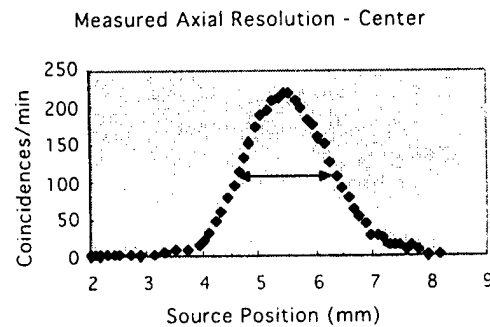
Figure 3: Axial response at field center measured by scanning a point source of ^{18}F in 0.1 mm steps. The FWHM = 1.75mm and the FWTM = 3.3m for the collimator gap used in the work presented here.

The system sensitivity was measured using 18F-filled cylinders of diameters from 0.5 to 4.5cm and a point source at the center of the field. The results for the cylinders are presented in figure 4 along with Montecarlo simulation results (solid line) for comparison. The point source sensitivity was measured to be 30 cps/uCi.
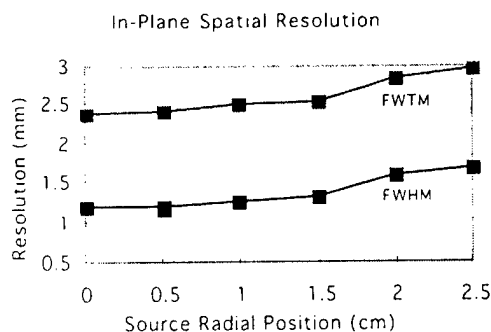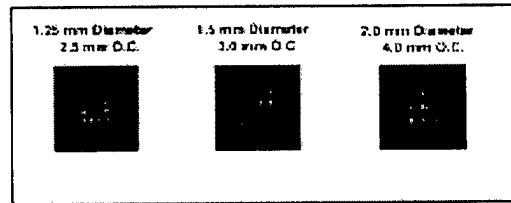

Figure 2a: Spatial resolution vs field radius measured with 0.45 mm diameter line sources of ^{18}F. Corrected for finite source diameter. The FWHM and FWTM are shown.
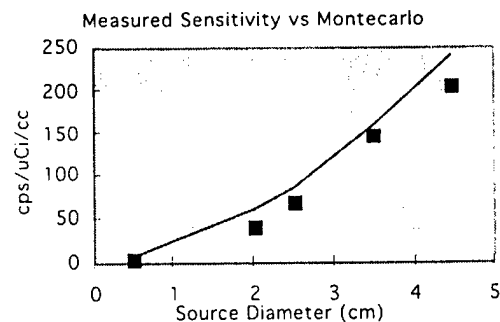

Figure 4: Measured sensitivity for cylindrical objects of varying diameter. The reported sensitivity includes all coincidence events above 150 keV. The solid line represents Montecarlo simulations of efficiency for 10 cm long cylinders under the same conditions.

The whole-field performance as a function of radioactivity concentration was measured using a 3cm diameter, 1cm long source of ^{13}N radioactivity. The measurements were made at the coincidence circuit output to eliminate the effects of the computer interface. The single channel events measured were the sum of all PMT timing signals and the coincidence rate measured includes all coincidences from within the central volume of the detector. The trues-data were corrected for randoms but not prompt scatter. Figure 5 shows the results of these measurements. The whole field rate at which randoms=trues is 60k trues/sec and little effect of deadtime was seen up to this rate. The singles/coincidence ratio was acceptably small over the whole range of the measurement.

From these data the noise equivalent countrate as a function of radioactivity in the field was computed incorporating the scatter estimate discussed below. The results, compared to the true coincidence rate, are shown in figure 6.

The linearity of reconstructed activity concentration in small objects was measured over a range of 0.1 to 20 uCi/cc. Arrays of five 3mm diameter cylindrical sources placed at 1cm radius in a 3.5 cm absorber were imaged, reconstructed and relative concentration measurements extracted from ROI's placed over the sources. Figure 7 shows a plot of These results.. The solid line is a linear least squares fit to the measured points. The system is shown to be linear over the range of the measurements with r^2 =0.96. Also shown is a sample image from the measurement. The dynamic range of the concentrations in this image is approximately 5 to 1.
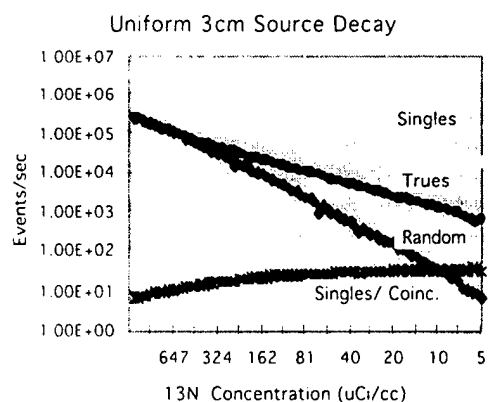
Uniform 3cm Source Decay

Figure 5: Measured whole field random coincidences, true coincidences, single events and single/coincidence ratio as a function of radioactivity concentration in a 3cm cylindrical object.
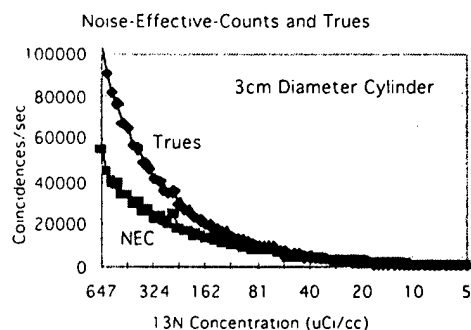
Noise-Effective-Counts and Trues

Figure 6. Noise equivalent count rate compared with true coincidence countrate up to randoms = trues for data presented in figure 5
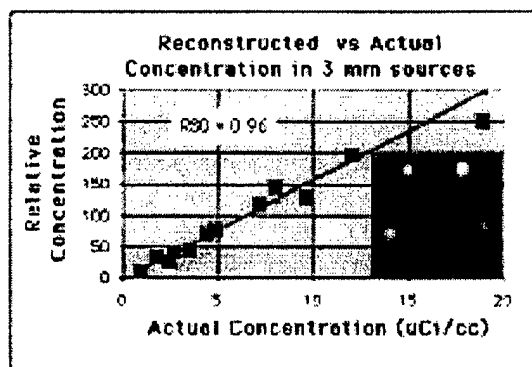

Figure 7: System linearity measured with arrays of five 3 mm diameter cylindrical sources located 1 cm from the field center. The sources were contained in a 3.5 cm diameter cylindrical absorber. The solid line is a linear least squares fit and the inset shows a sample image where the concentration dynamic range is 5 to 1.

The field uniformity of reconstructed data was measured in a 3.5cm-diameter uniform cylinder of ^{18}F radioactivity. 123 3mm circular ROI's were placed uniformly over the surface of the disk and relative-radioactivity-concentration values extracted. The variation in these values was found to be ± 5.4% (sample S.D.) and randomly distributed in an image with 3.5M coincidence events. The results are shown in figure 8.
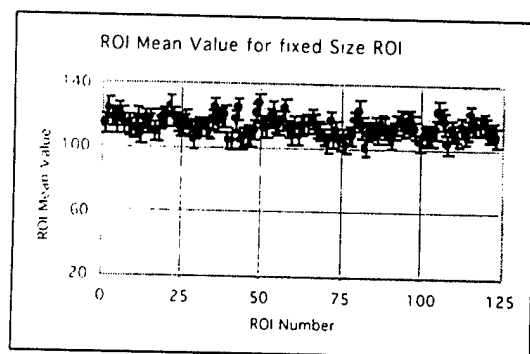
Figure 8 Field uniformity of a 3.5cm diameter cylindrical source sampled with 123.3mm diameter circular ROI's. The error bars are based on the sample standard deviation of ± 5.4%

The scatter fraction at the center of the imaging field was measured by placing a 0.45mm line source of ^{18}F surrounded by a 3.8cm diameter cylindrical polystyrene absorber at the center of the field. Data were collected at low countrate to minimize the effects of random coincidences. The sinogram of this object was integrated over all angles and the tails of the resulting data set (outside FWTM) were integrated to
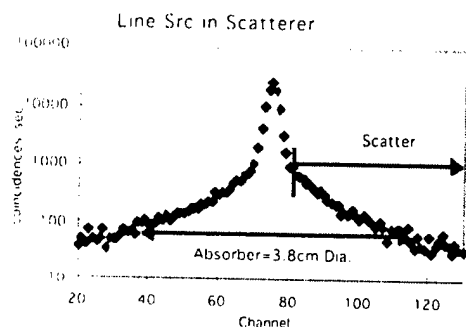

Figure 9 Integral over angle of sinogram of ^{18}F line source in 3.8cm polystyrene absorber located at field center. Scatter was defined as all events outside the FWTM of the peak. The scatter fraction is 5.7% as compared to a Montecarlo estimate of 7.1%.

provide an estimate of scatter. This was compared to the total integrated counts to give an estimate of the scatter fraction. The result, illustrated in figure 9, is that scatter fraction equals 5.7%. This compares fairly well with the value of 7.1% obtained by Montecarlo simulation.

In order to test the performance of the instrument under actual imaging conditions, a series of mouse imaging studies were carried out. Figure 10 shows a sequence of coronal brain images from a 25gm mouse

taken beginning 40 minutes after the injection of 2mCi of ^{18}F-FDG. The hemispheres are clearly distinguished and detail at the sub-hemispheric level can be seen. Figure 11 shows selected images from a mouse imaging study collected beginning 30 minutes after the injection of 1 mCi of ^{18}F-fluoride ion. A high degree of detail may be seen in the bone structure.
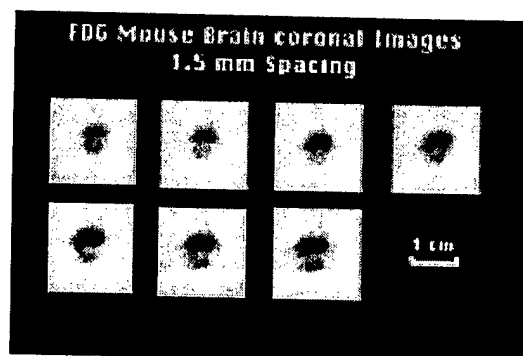

Figure 10: ^{18}F-FDG Images of mouse brain beginning 40 minutes after injection of 2 mCi of radioactivity. Each image was collected for approximately 20 minutes (1M events).
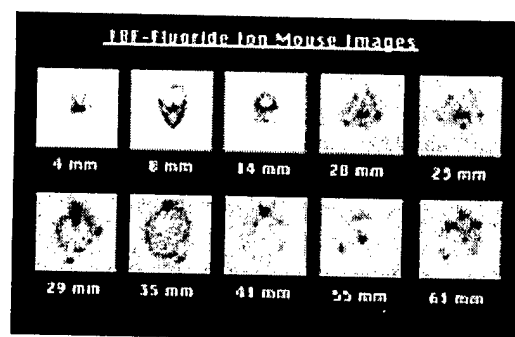

Figure 11: Selected ^{18}F-Fluoride images of mouse skeleton. Collection was begun approximately 30 minutes after the injection of 1 mCi or radioactivity. 0.25-0.5M events per image. The image positions are measured from the first plane near the nose.

IV. CONCLUSIONS

Performance measurements on a single-plane prototype PET instrument have been carried out. The purposes of these measurements were to characterize the instrument and to compile information for the design of a second generation device.

The measured in-plane spatial resolution, after correction for finite source size, is 1.17mm at the center of the field and varies up to 1.66mm at 2.5 cm radius.

These values are poorer than expected based on sampling considerations due in part to poor crystal identification at the block ends. This decreased resolution accounts for the fact that the measured resolution is fairly uniform over the central region of the field. The measured axial resolution of 1.75mm FWHM was obtained for the collimator used in the experiments presented here. By changing the collimator this resolution, as well as the inner diameter of the imaging aperture, may be varied; the range of slice thicknesses being limited on the low end only by system sensitivity and at the upper end by the 4.5mm crystal dimension. An alternative measurement of in-plane resolution, arrays of equi-spaced wells, indicates that high resolution (1.25mm) can be maintained in extended objects.

The system sensitivity for cylindrical objects and a point source at the center of the field agrees well with predictions from Montecarlo simulation although the measured sensitivities are systematically lower by about 20% in the cylinders and by 30% in the point source. The difference for the cylinders may be explained in part by the fact that poor light collection at the centers of the blocks gives rise to timing errors which result in the rejection of some good events. Both effects lead to underestimates of the sensitivity. In the case of the point source, small errors in source position may have a dramatic effect on the measured value and may account for the discrepancy.

The sensitivity is low due to two factors. The first is the use of detectors of limited radial dimension for the reasons stated above and the second is the need to limit events in a given crystal to a range of energies about the photopeak due to poor light collection from the center of the blocks. This process reduces the practical efficiency for useful events by 40-60% depending on the energy window-widths chosen.

The whole-system countrate measurements indicate that the system performs very well at high countrates showing little effect due to deadtime for activity concentrations up to about 800uCi/cc in a 2cm object. This is due in part to the fact that the data set generated is relatively small. The system is randoms limited and the point at which randoms=trues is 450uCi/cc (or alternatively 60,000 trues/sec). The robust behavior of the system in terms of randoms is explained by the highly restricted, single-plane, geometry.

Similarly, the scatter fraction measured with a line source at center-field surrounded by absorber yields a low result of 5.4% due to the restricted geometry. This result agrees fairly well with the 7.1% obtained from Montecarlo simulation.

Measurements of system linearity indicate that the system performs well over a range from 0.1-20 uCi/cc in small extended objects imbedded in absorber. Field uniformity in objects up to 3.5cm in diameter is about 5.4% (sample S.D.). This figure includes the effects of statistical fluctuations which, for the sizes or object and ROI's used in the measurements and the 3.5M events collected in the data set, is approximately 1.9% at the field center. The distribution of the fluctuations appears random.

The examples of mouse imaging studies shown demonstrate the resolution capabilities of the instrument as well as its limited sensitivity. The instrument may be effectively used for static imaging situations such as 18F-FDG imaging with moderate injected doses and may be useable, with larger injected doses, for some dynamic studies

The results of the studies presented here have led to several improvements which will be incorporated into a next generation device. These include: improved shielding design; improvements in block design particularly in terms of light output; redesign of the timing discriminator; and an improved PC interface.

V. ACKNOWLEDGMENTS

VI. REFERENCES

[1] Correia JA, Burnham CA , Kaufman D, et. al, "Small Animal PET imaging Device-Preliminary Design Study", *J. Nucl. Med.* 38:44P, 1997

[2] Correia JA, Burnham CA, Kaufman D, Fischman AJ, "Development of a Small Animal PET Imaging Device with Resolution Approaching 1 mm", *IEEE Transactions on Nucl.Sci.*, 46:631-635, 1999

[3] Melcher C.L. and Schweitzer J.S, "Cerium doped lutetium oxyorthosilicate: A fast, efficient new scintillator." *IEEE Transactions on Nucl. Sci.* , 39:502-505, 1992.

[4] Wong WH, Uribe J, Hicks K, et al, "A 2-dimensional detector decoding study on BGO arrays with quadrant sharing photomultipliers." *IEEE Transactions on Nucl. Sci.* NS41: 1453-1457, 1994

[5] Burnham CA., Elliott JT., Kaufman D., Chesler DA., Correia JA and Brownell G.L. "Single Interaction PET Detectors." *IEEE Transactions on Nucl Sci*, 37:832-835, 1990.

[authors]
J. CORREIA, C. BURNHAM, D. KAUFMAN, A..FISCHMAN
Massachusetts General Hospital, Harvard Medical School

[title]
DESIGNS FOR SMALL ANIMAL PET INSTRUMENTS
[text]
We have recently constructed a single plane PET imaging instrument with 1.2 mm spatial resolution. It consists of a 12.4 cm ring of 360 1 x 4.5 x 5mm LSO crystals organized into blocks of 12. Thin crystals were used to minimize photon-multiple-scatter in the detectors. This choice was necessary to obtain high spatial resolution and minimize the effects of inter-detector penetration, but it resulted in a considerable loss of sensitivity. This instrument has been used to image mice and small rats. The 1 mm resolution design-goal was not reached due to difficulties in identifying the outer crystals in the blocks and poor timing and low sensitivity at the centers of some blocks.

A second generation device which acknowledges the above limitations has been designed and is under construction. This device uses 10 1.2 mm crystals per block, each crystal being increased from 5 to 7 mm in depth. The detector ring diameter has been increased to 15 cm. Increasing crystal depth and ring diameter result in a net increase in sensitivity of 1.85, improved crystal identification, and better timing response. Preliminary results indicate that the new blocks will function consistently at 1.2mm resolution. Several designs for multi-planar blocks are also being studied.

[keywords]
PET; Instrumentation; Detectors
[topic]
501
[programme]
SCI
[preference]
EITHER

Design Considerations for Small Animal PET Device with Resolution Approaching 1mm.

J.A. Correia, C.A. Burnham, D. Kaufman, A.J. Fischman

Massachusetts General Hospital and Harvard Medical School, Boston, MA 02114

We have recently constructed a single-plane LSO-based-PET imaging instrument with 1.2 mm spatial resolution for imaging small animals. Thin crystals were used to minimize photon-multiple-scatter in the detectors. This choice was necessary to obtain high spatial resolution and minimize the effects of inter-detector penetration, but it resulted in a considerable loss of sensitivity. The 1 mm resolution design-goal was not reached due to difficulties in identifying the outer crystals in the blocks and poor timing and low sensitivity at the centers of some blocks.

A second generation device which addresses the above limitations has been designed and is under construction. This device uses ten 1.2 mm crystals per block, each crystal being increased from 5 to 7 mm in depth. The detector ring diameter has been increased to 14.5 cm. Increasing crystal depth and ring diameter result in a net increase in sensitivity of approximately 2.0, improved crystal identification, and better timing response. Preliminary results indicate that the new blocks will function consistently at 1.2mm resolution. Several designs for 3-dimensional blocks also are being studied with the eventual aim of construction a multi-planar device.

DRAFT

Design Considerations for Small Animal PET Devices with Resolution Approaching 1mm.

J.A. Correia, C.A. Burnham, D. Kaufman, A.J. Fischman

Massachusetts General Hospital and Harvard Medical School, Boston, MA 02114

I. INTRODUCTION

The purpose of the work reported here was to develop improved designs for the small-animal PET devices which are extensions of the 1 mm PET described previously [1, 2]. The existing system consists of a single 12 cm diameter ring with 360 LSO detectors viewed by 30 photo-multiplier tubes. Thin (5 mm) crystals and a low energy threshold were used to maximize the detection of single-interaction events and minimize inter-detector penetration for non-central lines of response. Crystals were identified using both position arithmetic and energy criteria.

This approach results in a considerable sacrifice in sensitivity in order to achieve high resolution. Sensitivity is limited by the low stopping power of the thin crystals and the need to reject many ambiguous events. Although the expected transverse resolution of this system, dictated by sampling, was 1 mm, the actual resolution obtained at center field was limited to approximately 1.2mm due to the fact that the crystals at the block ends were poorly identified. Further this device is limited by the fact that it images only a single plane.

II Redesigned Single-Plane Device

A device which addresses the above-stated limitations has been designed and is under construction. The main features of the design are given in Table 1. The differences from the prototype device, in addition to a new preamplifier design are:

1. Wider 1.2mm LSO crystal elements to give better block performance at 1.2mm resolution.
2. A larger detector array diameter of 14.5cm.
3. Crystal elements of 7mm depth to improve stopping power and hence sensitivity.
4. More phototube channels, 36 rather than 30, to accommodate the larger diameter.

5. Windows 95/98-based data acquisition interface which consists of a PCI data channel and a FIFO buffer to eliminate interface dead time.
6. Corrections for dead time, accidental coincidences and scattered photons leading to full quantitation.

PARAMETER	VALUE
Number of Planes	1
Detector Array Diameter	14.5 cm
Number of Crystals/Type	360/LSO
Crystal Dimensions	1.2 x 4.5 x 7mm
Number of Tubes/Blocks	36
In-Plane Resolution	1.25 mm center - 1.6 mm at 3cm
Axial Resolution	1.25 - 2.2 mm
Field of View	8 cm diameter
Point Source Sensitivity	70 coincidences/second/uCi

Table 1: Properties of new single-plane small animal PET.

III DETECTOR BLOCK DESIGNS

To-date several 10 crystal blocks have been constructed and tested using 7 mm deep crystals. The design of the blocks, similar to that of the prototype, is illustrated in figure 1a. The center six crystals are glued together and the outer two on each end of the block are separated by air gaps. The response of a typical test block to 511 keV photons is shown in figure 1b. This is a plot of the ratio spectrum computed from the PM tube signals ((A-B)/(A+B)). The ten crystals are clearly identified as compared to the previous block consisting of twelve 1mm wide crystals

which showed poorer identification of the end crystals.
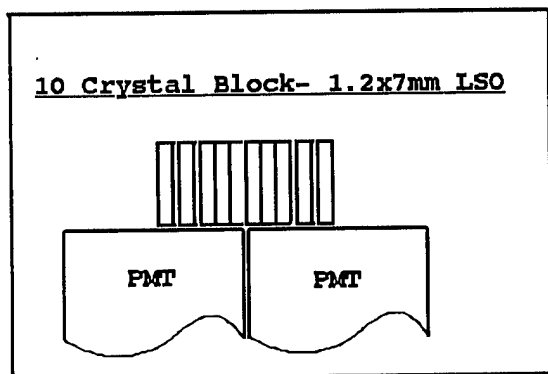

Figure 1a: Sketch of 2-dimensional block consisting of ten 1.2x4.5x7mm LSO crystals. The central six crystals are glued together and the outside two on each side are separated by air gaps.
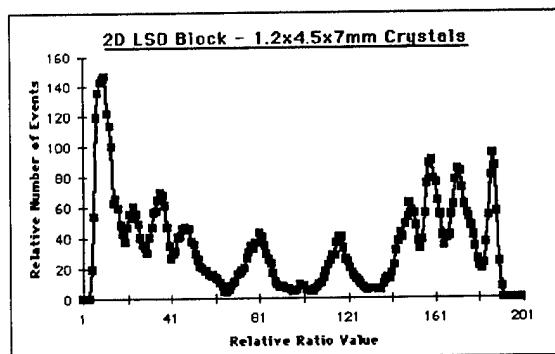

Figure 1b: Measured ratio spectrum of 10 element 2-D block consisting of 1.2x4.5x7mm LSO crystals.
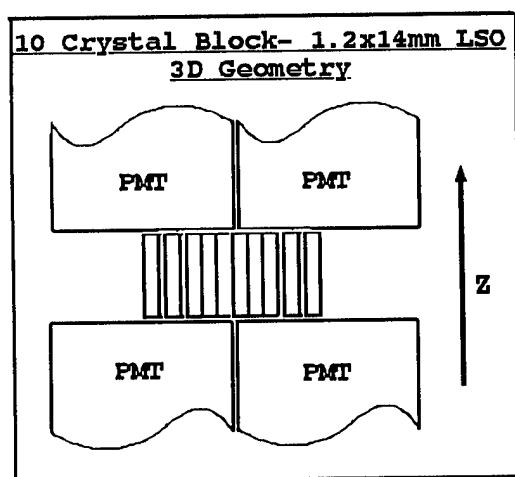

Figure 2: 3-D Block design consisting of ten 1.2 mm wide x 7mm deep x 14mm high(z) LSO crystals viewed by 2 PMTS at each end. Surfaces are as in 2-D block.

In order to further improve sensitivity, an attempt is underway to design a 3-dimensional block which could be used as the basis for a multi-planar or volumetric device having resolution similar to the 2-dimensional device. Exploration of several designs is proceeding simultaneously. One of the more promising is illustrated in figure 2. This design collects light from both ends of 14 mm long LSO crystals and in addition to a crystal identification calculation, uses the balance of light between the top and bottom of the block to establish a z-coordinate for each event. Several variants of this design which use different phototube locations (e.g., at the back of the array) are also being explored.

IV. CONCLUSIONS

An improved single-plane, small animal device has been designed and is under construction. Initial experiments with 10-crystal blocks indicate that crystal identification will be considerably improved compared to our present system. The use of deeper 7mm crystals results in improved sensitivity while increasing the ring diameter to 14.5 cm keeps depth-of-interaction degradation approximately the same as that in the prototype instrument. The net sensitivity is increased by approximately a factor of two. Several 3-D block designs are also being explored and their implementation will result in an additional large improvement in system sensitivity.

REFERENCES

[1] Correia JA, Burnham CA, Kaufman D, Fischman AJ, "Development of a Small Animal PET Imaging Device with Resolution Approaching 1 mm.", *IEEE Transactions on Nucl. Sci.* 45:631-635, 1999.

[2] Correia JA, Burnham CA, Kaufman D, Fischman AJ, "Performance of a Small Animal PET Instrument with 1 mm Resolution.", *IEEE Medical Imaging Conf, Conference Record.*, 1999.